- 1 Rapid southeastern Laurentide Ice Sheet thinning during the last deglaciation revealed by
- 2 elevation profiles of *in-situ* cosmogenic <sup>10</sup>Be

- 4 Christopher T. Halsted<sup>1,2</sup>, Paul R. Bierman<sup>1,2</sup>, Jeremy D. Shakun<sup>3</sup>, P. Thompson Davis<sup>4</sup>, Lee B.
- 5 Corbett<sup>1</sup>, Marc W. Caffee<sup>5</sup>, Taylor Hodgdon<sup>6</sup>, Joseph Licciardi<sup>6</sup>
- 6 <sup>1</sup> Rubenstein School of Environment and Natural Resources, University of Vermont, 81 Carrigan
- 7 Dr, Burlington, VT 05405
- 8 <sup>2</sup> Gund Institute for Environment, University of Vermont, 210 Colchester Ave, Burlington, VT
- 9 05405
- <sup>3</sup> Department of Earth and Environmental Sciences, Boston College, 140 Commonwealth
- 11 Avenue, Chestnut Hill, MA 02467
- <sup>4</sup> Department of Natural and Applied Sciences, Bentley University, 175 Forest St, Waltham, MA
- 13 02452
- <sup>5</sup> Department of Physics and Astronomy, Purdue University, 525 Northwestern Ave, West
- Lafayette, IN 47907
- <sup>6</sup> Department of Earth Sciences, University of New Hampshire, 56 College Road, Durham, NH
- 17 03824

18

19

#### **ABSTRACT**

- Accurate reconstruction of Laurentide Ice Sheet volume changes following the Last
- 21 Glacial Maximum is critical for understanding ice sheet contribution to sea-level rise, the
- resulting influence of meltwater on ocean circulation, and the spatial and temporal patterns of
- 23 deglaciation. Here, we provide empirical constraints on Laurentide Ice Sheet thinning during the

last deglaciation by measuring *in-situ* cosmogenic <sup>10</sup>Be in 81 samples collected along vertical transects of nine mountains in the northeastern United States. In conjunction with 107 exposure age samples over five vertical transects from previous studies, we reconstruct ice sheet thinning history.

At peripheral sites (within 200 km of the terminal moraine), we find evidence for ~600 m of thinning between 19.5 and 17.5 ka, coincident with the slow initial margin retreat indicated by varve records. Further up-ice (>400 km north of the terminal moraine), exposure ages above and below 1200 m a.s.l. exhibit different patterns. Ages above this elevation are variable and older, while lower elevation ages are indistinguishable over 800-1000 m elevation ranges, suggestive of a subglacial thermal boundary ~1200 m a.s.l. separating erosive, warm-based ice below and polythermal, minimally-erosive ice above. Low-elevation ages from up-ice mountains are between 15 and 13 ka, suggesting rapid thinning of ~1000 m coincident with Bølling-Allerød warming. This rapid paleo-ice thinning is comparable to rates from other vertical exposure age transects around the world and may have been faster than modern basin-wide thinning rates in Antarctica and Greenland, suggesting that the southeastern LIS was highly sensitive to a warming climate.

#### INTRODUCTION

Thinning rates of major Northern Hemisphere ice sheets following the Last Glacial Maximum (LGM) are not well constrained and represent a key uncertainty in reconstructions of land-ice volume changes and the contribution of melting ice to global sea-level rise (SLR). Even as SLR reconstructions have become more sophisticated (Lin et al., 2021), the partitioning of SLR contribution from individual LGM ice sheets over time remains uncertain (Lambeck et al., 2014). The volume and timing of ice loss from LGM ice sheets are essential data for simulations

of future ice sheet mass loss, which rely on ice sheet reconstructions to estimate climate sensitivity of modeled ice sheets (Stokes et al., 2015). Meltwater input to oceans from ablating ice sheets can also have an outsized effect on regional and global climates (Clark et al., 2001; Clark et al., 2012) so accurate estimates of meltwater inputs over time contribute to a more detailed understanding of deglacial paleoclimate dynamics (Tarasov and Peltier, 2005).

Changes in ice sheet areal extent have been investigated using a variety of geochronological methods. Although some LGM ice sheets have hundreds to thousands of age constraints informing extent reconstructions (Stroeven et al., 2016; Clark et al., 2018; Dalton et al., 2020), data constraining ice sheet thickness changes over time remain sparse. The availability of minimum-limiting radiocarbon ages for deglacial chronologies is generally limited outside lowland areas (e.g., Dalton et al., 2020), precluding their use for constraining ice thinning rates. Using inversion techniques, ice thickness can be inferred from rates of glacial isostatic adjustment in regions formerly covered by ice sheets (e.g., Peltier et al., 2015; Lambeck et al., 2017), although these models rely on assumed values for mantle viscosity that are uncertain, resulting in model disagreements (Clark and Tarasov, 2014). Likewise, physical ice sheet models attempt to reconstruct paleo-ice sheet thickness using areal extent constraints and extent-height relationships observed in modern ice sheets (e.g., Gowan et al., 2021), but there is significant uncertainty about the extent-height relationship in ablating ice sheets with a negative mass-balance (Gregoire et al., 2012; Abe-Ouchi et al., 2015).

Cosmogenic-nuclide exposure age 'dipsticks' empirically constrain ice sheet thinning in areas with topographic relief and represent a way to address the lack of robust measures of ice thinning over time. These dipsticks use exposure ages from *in situ* cosmogenic nuclides measured along an elevation transect, allowing temporal reconstruction of a lowering paleo-ice

surface (e.g., Stone et al., 2003). Exposure age dipsticks have been used to constrain ice thinning histories of the Greenland (e.g., Winsor et al., 2015), Fennoscandian (e.g., Brook et al., 1996; Goehring et al., 2008), and Antarctic (e.g., Stone et al., 2003; Mackintosh et al., 2007; Johnson et al., 2014; Small et al., 2019) ice sheets. In this study, we collected samples along vertical transects of mountains in the northeastern United States (U.S.) and constructed eight new exposure age dipsticks (Fig 1) that date the thinning of the southeastern Laurentide Ice Sheet (LIS), which contributed the most volume to SLR of any ice sheet during the last deglaciation (Tarasov et al., 2012; Clark and Tarasov, 2014). This project is a continuation of ongoing efforts to reconstruct deglacial ice thickness changes in the northeastern U.S. (Table 1; Davis et al., 2015; Koester et al., 2017; Barth et al., 2019; Corbett et al., 2019; Koester et al., 2020), which is the only region along the southern margin of the LIS with topography sufficient to make such measurements. We use these dipsticks to infer when and how rapidly thinning occurred and speculate about possible drivers of ice loss.

#### **BACKGROUND**

# In situ Cosmogenic Nuclide Exposure Dating

In situ cosmogenic nuclides, particularly <sup>10</sup>Be in quartz, have been used extensively to define deglacial chronologies around the world (Balco, 2011). Warm-based, erosive ice that covers the landscape for thousands of years can effectively remove many meters of bedrock and thus nuclides produced mostly near the surface (≤2 m depth) during prior periods of exposure (e.g., Nishiizumi et al., 1989). Assuming that post-glacial erosion and cover by snow or till are negligible for sampled surfaces (Phillips et all, 1990; Ivy-Ochs and Kober, 2008), the duration of exposure following glacial retreat is estimated by measuring <sup>10</sup>Be concentrations (Nishiizumi et al., 1991; Ivy-Ochs et al., 1995; Steig et al., 1998; Bierman et al., 1999). Short ice occupation

times and/or cover by non-erosive, cold-based ice can allow nuclides from prior periods of exposure to remain after ice retreats (Bierman et al., 1999; Briner et al., 2005), and the most recent postglacial exposure duration will be over-estimated (e.g., Bierman et al., 2015; Corbett et al., 2019; Koester et al., 2020). Post-glacial cover will partially or completely shield surfaces from cosmic radiation and result in under-estimation of exposure durations (Schildgen et al., 2005; Heyman et al., 2011).

#### **Existing Deglacial Constraints in the Northeastern United States**

The northeastern U.S. has a long history of glacial chronology research, although the vast majority of this work has focused on the timing of ice margin retreat instead of ice thinning. The initial retreat of the LIS from its terminal moraines in the northeastern U.S. was slow and occurred during the early deglacial period (Stanford et al., 2020). Deglaciation constraints from bog- and lake-bottom sediment core radiocarbon ages and <sup>10</sup>Be exposure ages disagree substantially at locations near (<150 km) the terminal moraine (Balco and Schaefer, 2006; Peteet et al., 2012). At these peripheral locations, ages from neither method are likely to reflect the true timing of deglaciation (Halsted et al., 2021). The timing and duration of the local glacial maximum in the northeastern U.S. is better constrained to approximately 26 to 24 ka on the basis of pre-LGM radiocarbon ages from sites outboard of the ice margin (Sirkin and Stuckenrath, 1980) and a calibrated varve chronology (Stanford et al., 2020). Ice margin retreat began after 24 ka and continued at a slow rate of 10 to 30 m/yr (Ridge et al., 2012; Stanford et al., 2020) until 18 ka, interrupted by several stand-stills or re-advances as indicated by recessional moraines (Balco and Schaefer, 2006).

After 18 ka, when the LIS margin had retreated more than 150 km from the terminal moraine, abundant deglacial ages from multiple different dating methods agree well and indicate

continuous retreat through the northeastern U.S. with a brief stand-still or re-advance around 14 ka (e.g., Ridge et al., 2012; Bromley et al., 2015; Thompson et al., 2017). The pace of ice margin retreat remained slow from 18 to 16 ka (30 to 40 m/yr), increased to ~90 m/yr from 16 to 14.6 ka, and accelerated to 300 m/yr after 14.6 ka (Ridge et al., 2012). The LIS margin was north of the White Mountains in northern New Hampshire by 14 ka (Bromley, 2015; Thompson, 2017) and had retreated north across the modern U.S./Canada border by 13 ka (Fig 1; Ridge et al., 2012; Dalton et al., 2020).

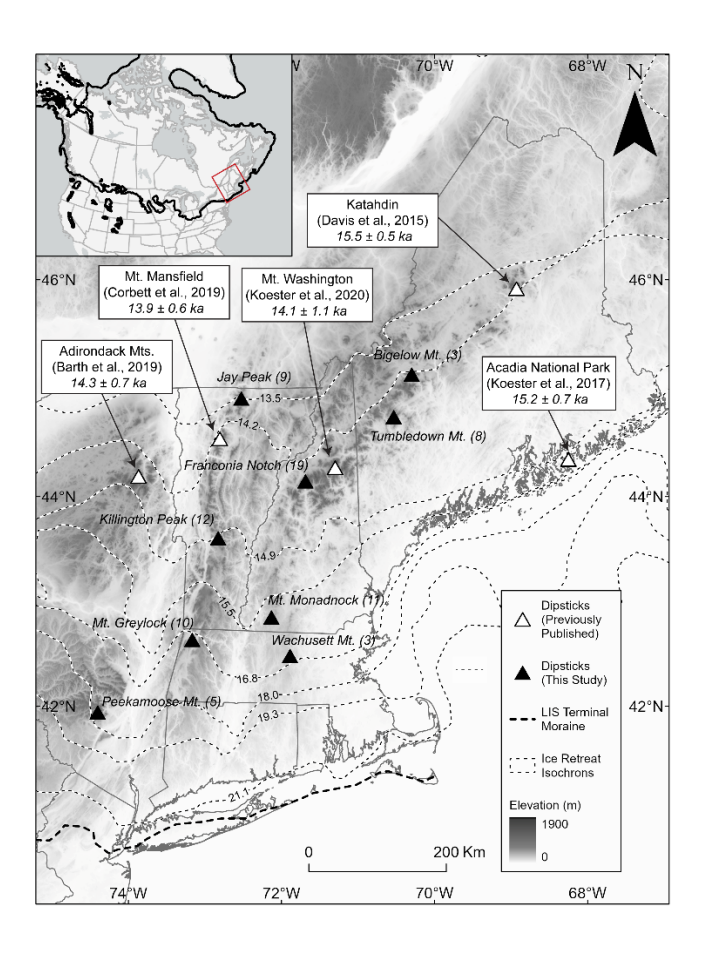


Figure 1: Topography and deglacial constraints in the northeastern U.S. Thin dashed lines on main map show ice margin positions at times in ka during the deglacial period (based on Ridge et al., 2012, and Dalton et al., 2020). Inset shows the Laurentide Ice Sheet at its maximum extent, including its coalescence with the Cordilleran, Innuitian, and Greenland ice sheets with box on inset map showing extent of main map. Numbers in parentheses next to dipstick labels are the number of samples with data at each location.

Cosmogenic data constraining ice thinning in the northeastern U.S. have been previously collected at five widely separated sites once occupied by the LIS (Fig 1, Table 1). Ice thinning and retreat in coastal Maine occurred at  $15.2 \pm 0.7$  ka (Koester et al., 2017), coincident with exposure ages from Katahdin in west-central Maine (16 to 15 ka; Davis et al., 2015). Exposure age dipsticks indicate similar timing for ice thinning on Mount Washington in northern New Hampshire (average age  $14.1 \pm 1.1$  ka; Koester et al., 2020) and Mount Mansfield in northern Vermont (13.9  $\pm$  0.6 ka; Corbett et al., 2019). Measured <sup>10</sup>Be concentrations from the highest sampled elevations in New Hampshire (>1600 m a.s.l.) and Vermont (>1200 m a.s.l.) are variable and some are far higher than low-elevation samples, suggesting nuclide inheritance from earlier exposure. Geomorphic evidence of ice cover and analysis of short-lived in situ <sup>14</sup>C in some of the high-elevation samples indicate that these high peaks were covered by minimallyerosive ice at the LGM and were likely exposed before 18 ka (Bierman et al., 2015; Corbett et al., 2019; Koester et al., 2020). A dipstick constructed in the Adirondack Mountains of northern New York (Barth et al., 2019) relies on whole rock <sup>36</sup>Cl exposure ages. The <sup>36</sup>Cl ages suggest slow initial thinning of the upper peaks (>1300 m a.s.l.) from 20 to ~16 ka followed by rapid thinning over the remainder of sampled elevations from 16 to 13 ka (Barth et al., 2019).

130

131

132

133

134

135

136

137

138

139

140

141

142

143

144

145

TABLE 1: PREVIOUSLY-PUBLISHED DIPSTICKS IN THE NORTHEASTERN U.S.\*

Location	Number of samples	Elevations (m a.s.l.)	Time of ice thinning (ka)	Source
Acadia National Park, Me. (44.3, -68.2)	24	81 - 460	$15.2 \pm 0.7$	Koester et al. (2017)
Katahdin, Me. (45.9, -68.9)	13	744 - 1598	$15.5 \pm 0.5$	Davis et al. (2015)
Mt. Mansfield, Vt.** (44.5, -72.8)	20	409 - 1305	$13.9 \pm 0.6$	Corbett et al. (2019)
Mt. Washington, N.H. <sup>†</sup> (41.3, -71.3)	20	656 - 1907	$14.1 \pm 1.1$	Koester et al. (2020)

	Adirondacks N.Y.§ (44.2, -73.9)	21	403 - 1560	$14.3\pm0.7$	Barth et al. (2019)		
147 148 149 150 151 152	elevation samples from Mt. Washington and Katahdin published in Bierman et al. (2015)  **Evidence of inherited <sup>10</sup> Be above 1200 m a.s.l Time of ice thinning from n = 15 samples below 1200 m a.s.l.  †Evidence of inherited <sup>10</sup> Be above 1600 m a.s.l Time of ice thinning from n = 9 samples below 1600 m a.s.l.  §Exposure ages from <sup>36</sup> Cl. Time of ice thinning from n = 9 samples below 1300 m a.s.l.						

# **METHODS**

# **Experimental Design**

We assume that mountains in the northeastern U.S. became exposed in a top-down pattern as the LIS thinned, becoming nunataks with bare summits (i.e., without remnant ice caps covering peaks) as the ice surface lowered around them. By calculating <sup>10</sup>Be exposure ages along a vertical transect of a mountain, we aim to determine the progressive exposure of the land surface as the ice ablates and thins (Fig 2).

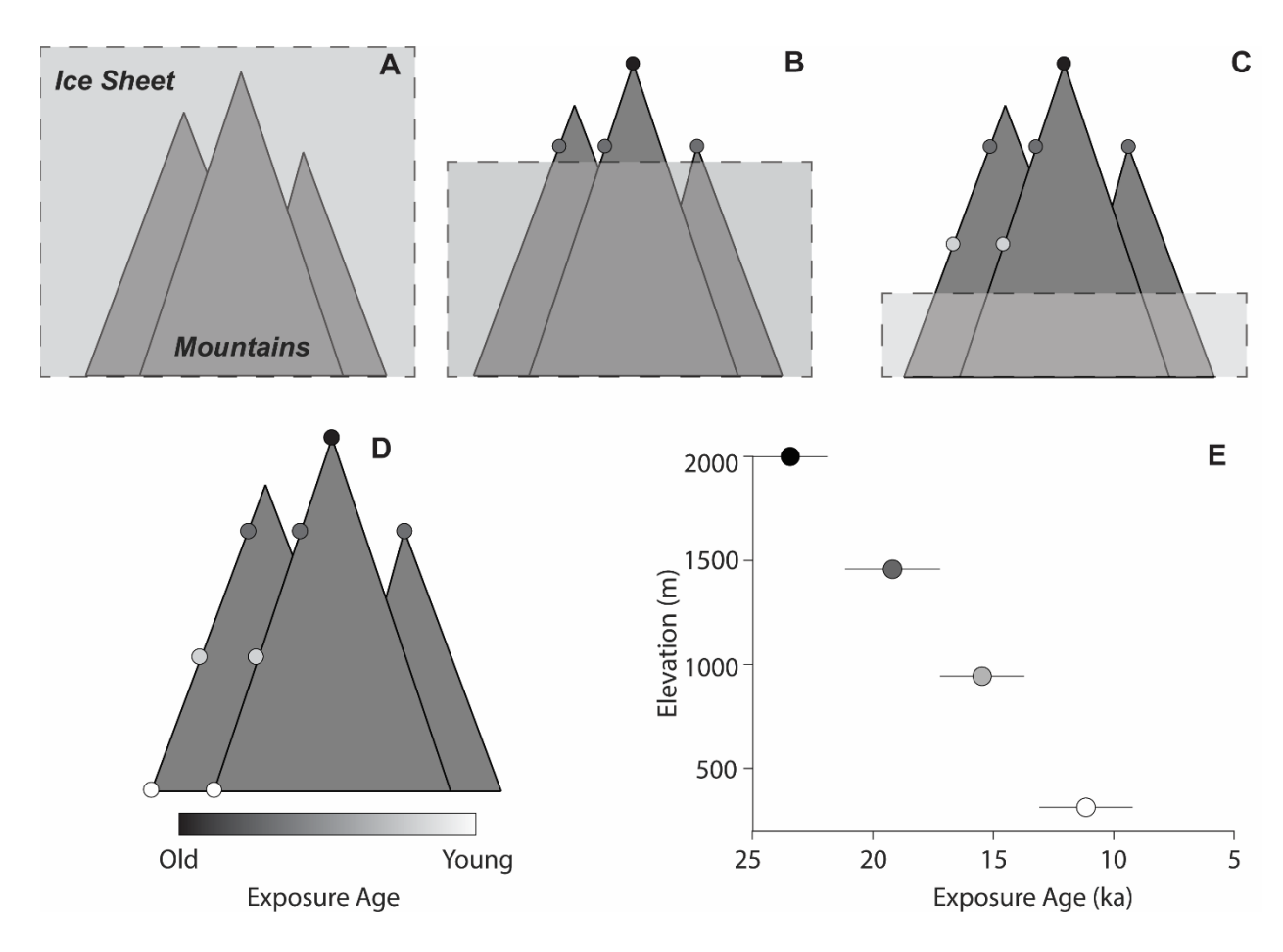


Figure 2: Conceptual illustration of the dipstick approach. Figure modified from (Bierman et al., 2021). In all panels, circles represent exposure ages of samples following the grayscale scheme in panel (D). Panels (A-C) show an ice sheet lowering around the mountains, progressively exposing lower elevations over time as ice thins. Panel D shows the expected pattern of in situ cosmogenic nuclide exposure ages, an increase in exposure age with elevation on the deglaciated mountains. Panel E schematically shows the typical depiction of these data: a plot of <sup>10</sup>Be-based exposure age and uncertainty on the x-axis and sample elevation on the y-axis. Regressions of these elevation-exposure age data reveal trends that represent rates of ice sheet thinning over time.

#### **Field Methods**

We sampled boulders with indications of glacial transport and bedrock outcrops with indication of glacial erosion for exposure age determination. We preferentially sampled boulders more than 1 m high because their top surfaces are less likely to have experienced post-glacial surficial cover than bedrock; exposure ages from large boulders may thus better reflect local deglaciation age (Heyman et al., 2016). To further maximize the likelihood that exposure ages

from sampled boulders reflect local deglaciation timing and not postglacial mass movement, we used sampling criteria including sub-angular to rounded shape (indicative of englacial transport and erosion), perched locations on local high points in the topography, and, when possible, we sampled lithologies differing from the local bedrock.

We sampled the top few centimeters of boulders and bedrock and recorded site and sample parameters (lithology, topographic shielding, surface strike/dip, sample thickness) for exposure age calculations. We recorded the strike and dip of the sampling surface using a Brunton compass and used a chisel and hammer to collect each sample. We used Garmin eTrex® 20 and GPSMap 60CSx GPS units with ≤3 m location accuracy to record latitude, longitude, and elevation and used an inclinometer to evaluate shielding due to topographic features surrounding the sampling site. We provide site information for all samples in the GSA Data Repository.

# **Laboratory Methods and Isotopic Analysis**

We processed all but four samples for exposure dating at the University of Vermont using weak acid etching to isolate and purify quartz (Kohl and Nishiizumi, 1992) and established methods to extract Be (Corbett et al., 2016; see GSA Data Repository for analytical information related to sample processing). Four samples from Mount Monadnock, New Hampshire, were processed in the cosmogenic isotope clean lab at the University of New Hampshire following lab methods similar to those described above. We measured <sup>10</sup>Be/<sup>9</sup>Be ratios by accelerated mass spectrometry (AMS) at the Purdue Rare Isotope Measurement Laboratory (PRIME; samples prepared at University of Vermont) and at the Center for Accelerator Mass Spectrometry at Lawrence Livermore National Laboratory (CAMS-LLNL; samples prepared at University of New Hampshire). <sup>10</sup>Be AMS measurement precisions have a right-skewed distribution with most samples between 1.6 to 5.6% precision (median ± 1σ), but with a few high outliers including 8.9

and 10.0%. We corrected the measured sample <sup>10</sup>Be/<sup>9</sup>Be ratios for backgrounds by subtracting the average <sup>10</sup>Be/<sup>9</sup>Be blank ratio from all batches (treating the University of Vermont and University of New Hampshire samples separately), then propagated the uncertainties in quadrature (see GSA Data Repository).

#### **Age Calculations**

We calculated exposure ages using version 3 of the online exposure age calculator described by Balco et al. (2008), LSDn scaling (Lifton et al., 2014), and a regional <sup>10</sup>Be production rate calibration data set for northeastern North America (Balco et al., 2009). We use the Balco et al. (2009) calibration data set to increase the precision of calculated exposure ages and because the regional calibration data set inherently accounts for changes in <sup>10</sup>Be production rates over the Holocene due to postglacial isostatic uplift, as the calibration samples experienced grossly similar uplift histories as our exposure age samples. All samples were assigned densities between 2.6 to 2.8 g/cm<sup>3</sup>, values appropriate for the predominately granite, schist and quartzite sample lithologies. Calculated exposure ages assume no inherited <sup>10</sup>Be from prior exposure, no post-exposure erosion, and no shielding due to snow or vegetation.

We report two uncertainties with each exposure age in the GSA Data Repository: analytical uncertainties ('internal') and uncertainties due to both analytical processes and nuclide production estimation and scaling schemes ('external'). We use internal uncertainty when comparing <sup>10</sup>Be ages within the same dipstick (i.e., for interpreting thinning pace) because samples come from a relatively small geographic area so errors in production rate calibration or scaling are highly correlated between samples. We use external uncertainty when comparing our <sup>10</sup>Be exposure ages to previously-published deglacial chronologies. Incorporating <sup>10</sup>Be production rate uncertainties is needed when comparing exposure ages across nuclides—such as

<sup>36</sup>Cl ages from the Adirondack Mountains (Barth et al., 2019)—or comparing exposure ages to deglacial constraints from different methods such as calibrated glacial varve chronologies and core-bottom radiocarbon ages.

#### TRANSECT SITES AND SAMPLING STRATEGY

The northeastern U.S. is characterized by inland mountain ranges in which the highest elevations (>1200 m a.s.l.) exhibit signs of minimal glacial erosion due to cold-based ice cover during glacial periods, as informed by multiple-nuclide analyses and geomorphic evidence of preserved landscapes, while lowland valleys were deeply scoured by glaciation (Bierman et al., 2015; Corbett et al., 2019; Koester et al., 2020). LIS retreat chronologies in these inland locations predominately come from the lowlands, which contain abundant glacial-lacustrine sediment (Ridge et al., 2012), ice-contact deposits (Thompson et al., 1999), a few isolated recessional moraines (Davis, 1989; Bromley et al., 2015; Thompson et al., 2017; Bromley et al., 2019), and dozens of ponds and bogs with basal <sup>14</sup>C ages (Halsted et al., 2021).

Eight new transects reported here are located on prominent mountains spread throughout the region (Fig 1, Table 2), maximizing spatial coverage. We provide descriptions of each transect site in the following sections, while location, site parameter information (sample type, topographic shielding, sample thickness), and field photos for each sample are provided in the GSA Data Repository. The steep flanks of Bigelow Mountain limit the availability of suitable boulder samples and we therefore construct a transect in northwestern Maine composed of samples from both Bigelow and Tumbledown Mountains (located ~40 km apart). LIS retreat chronologies suggest that these mountains were deglaciated within a century or two of each other (Fig 1; Dalton et al., 2020), well within the analytical uncertainty of exposure age measurements and therefore indistinguishable within the resolution of our deglacial chronometer.

TABLE 1: VERTICAL TRANSECT SUMMARIES AND RELATION TO TERMINAL MORAINE OF LIS

Dipstick Location	Number of Samples	Sample Elevation Range (m a.s.l.)	Distance to Terminal Moraine (km)
Peekamoose Mtn., N.Y. (41.953N, 74.398W)	5	900 – 1170	145
Wachusett Mtn, Mass. (42.503N, 71.886W)	3	370 – 560	180
Mt. Greylock, Mass. (42.638N, 73.166W)	10	390 – 1060	210
Mt. Monadnock, N.H. (42.861N, 72.108W)	11	420 – 960	220
Killington Peak, Vt. (43.605N, 72.820W)	12	490 – 1290	315
Franconia Notch, N.H. (44.142N, 71.681W)	19	590 - 1600	350
Tumbledown Mtn., Me.* (44.751N, 70.547W)	8	850 - 1050	390
Bigelow Mtn., Me.* (45.147N, 70.289W)	3	500 - 1250	430
Jay Peak, Vt. (44.965N, 72.460W)	9	570 - 1170	460

\*Samples from Tumbledown and Bigelow Mountains are combined into one transect for northwestern Maine

# 

# Peekamoose Mountain (Catskill Mountains), New York

The Catskill Mountains of southern New York are an uplifted, dissected plateau of primarily Devonian age siliciclastic sedimentary rocks (Ver Straeten, 2013). Our transect site is in the eastern Catskills, where glacially transported conglomerate boulders contain embedded quartz pebbles 2 to 6 cm in diameter. We collected five samples from Peekamoose Mountain. Three samples (CAT-01, 02, 03) were collected from the summit area, all with elevations greater than 1100 m a.s.l., and two samples (CAT-04, 05) were collected below the summit at ~900 m a.s.l. Each sample consisted of several quartz pebbles embedded at the surface of conglomerate boulders. We assume that each pebble had similar exposure histories to its neighbors on the surface of the boulders, and together they are treated as single samples.

#### Wachusett Mountain, Massachusetts

Wachusett Mountain is part of the Fitchburg plutonic complex, a series of metamorphosed igneous sheets in central Massachusetts and southern New Hampshire (Zen et al., 1983). At 611 m a.s.l., Wachusett Mountain is the highest point in the Fitchburg complex, which is otherwise characterized by rolling hills reaching no more than ~400 m a.s.l.. With a vertical relief of 306 m, Wachusett Mountain captures only a brief window in the southeastern LIS thinning history. Wachusett's value is in its location; it is the highest peak in central Massachusetts and is surrounded by mostly low relief terrain, making it the only location to construct a dipstick in southeastern New England. Three samples were collected from Wachusett Mountain in roughly 60 m elevation increments. Two samples are from large boulders composed of local gneiss (WSP-02, 05), and the other sample is a smoothed bedrock outcrop (WSP-04). We did not collect a summit sample from Wachusett Mountain because of human landscape disturbance.

# Mount Greylock (Taconic Mountains), Massachusetts

Mount Greylock is part of the Taconic Mountains of southwestern Vermont but is located near, and typically associated with, the Berkshire Mountains of northwestern Massachusetts. Greylock is the tallest mountain in the state, with a summit elevation of 1064 m a.s.l. and a vertical relief of 751 m. Mount Greylock is composed of Ordovician schist and phyllite of the Taconic allochthon which was thrust over lower Cambrian schist during the Taconic orogeny (Ratcliffe et al., 1993). Nine samples were collected from Mount Greylock. MG-01 and -02 are from boulders near the summit composed of the Ordovician phyllite characteristic of the upper reaches of the mountain. MG-03, -04 (Fig 3), and -06 are from bedrock quartz veins near the summit. MG-05 and -07 are from boulders midway down the mountain and are also composed of

local phyllite. MG-08 and -09 are from large quartzite boulders located to the north of Mount Greylock, at around 400 m a.s.l. These boulders were probably sourced from quartzite outcrop located more than 100 m away across flat terrain, suggesting that the boulders were quarried and transported by glaciers rather than rolling downslope during the Holocene.

#### Mount Monadnock, New Hampshire

Mount Monadnock is the tallest peak in southern New Hampshire, with a summit elevation of 965 m a.s.l. and a vertical relief of 650 m. The bedrock is schist and quartzite of the Devonian Littleton Formation (Lyons et al., 1997). We collected 11 samples along a vertical transect of Mount Monadnock. MON-01, 02, and 03 are from a boulder-rich area on rolling, low-slope topography near the base of the mountain (~400 m a.s.l.), suggesting an eroded till landscape rather than a landslide deposit. MON-04 (420 m a.s.l.) and 08 (520 m a.s.l.) are isolated boulder samples away from the basal boulder-rich area. All boulder samples are composed of native schist lithology. MON-05 and 06 are bedrock samples located higher on the mountain (794 and 710 m a.s.l., respectively). NH15-16, 17, 18, and 19 were collected from ice-scoured bedrock at ~960 m a.s.l. near the summit of Mount Monadnock (Hodgdon, 2016). All four bedrock samples collected near the summit are from quartz veins that exhibit abundant striae.

#### Killington Peak (Green Mountains), Vermont

Killington is the tallest mountain in southern Vermont, with a summit elevation of 1288 m a.s.l., and is part of the Green Mountain range, which runs north-south for the entire length of Vermont. The bedrock of Killington Peak is part of the Mount Holly Complex, a middle Proterozoic paragneiss unit intruded by late Proterozoic pegmatites (Walsh and Ratcliffe, 1994). We collected 12 samples along a vertical transect of Killington Peak. Four of the samples (KM-

01 through-04) are from prominent bedrock quartz veins near the exposed summit, while five samples collected along the flank of Killington (KM-05 through -09) come from boulders of native lithology. Samples KM-05 and KM-06 were collected from the steep (15-20°) upper slopes, whereas samples KM-07 and -08 came from lower elevations, where the slope is gentler (5-10°). Sample KM-09 was taken from a boulder located in a flat area at the base of Killington. Sample KM-10 (Fig 3) is a bedrock sample from the top of a hill (Deer Leap Lookout) ~1 km away from the Killington base. Samples KM-11 and -12 are two samples from erratic boulders about 2 km distal from Killington.

#### Franconia Notch (White Mountains), New Hampshire

Franconia Notch is a glacially-carved valley in the western White Mountains of New Hampshire. The bedrock of the deeply-scoured lower elevations of Franconia Notch is middle Jurassic Conway granite, a coarse-grained unit with a characteristic pink color (Lyons et al., 1997). The high mountain ridge on the eastern side of the notch is composed of early Jurassic Lafayette granite porphyry that is part of a remnant ring dike (Allen et al., 2001), and the western ridge of the notch is underlain by the early Devonian Kinsman granodiorite. We collected 16 samples in Franconia Notch at an elevation range between 590 m and 1600 m a.s.l.. The Franconia samples come from several locations in the notch, including Mount Lafayette (LFT and PTD; Fig 3), Mount Lincoln (FW and FR), Artist's Bluff (AB), Lonesome Lake (LL), and the valley floor (FN). Most of the samples are from boulders but a few were collected from bedrock outcrops (LFT-17, LFT-14, and LFT-13).

#### **Tumbledown Mountain, Maine**

Tumbledown Mountain in western Maine has three distinct, rounded peaks at elevations between 875 and 1060 m a.s.l. surrounding an alpine pond. The bedrock is primarily greenschist

and other fine-grained metasedimentary units of the Silurian Perry Mountain formation (Osberg et al., 1985; Moench and Pankiwskyj, 1988). Stoss/lee features, grooves, and glacially-molded bedrock are abundant on the exposed summit of Tumbledown Mountain. We collected eight samples from Tumbledown Mountain. Two boulder samples are from the base of the mountain (TM-07 and 08), and three other boulder samples (TM-04, 05, 06; Fig 3) come from different elevations up the mountain slope to the summit. TM-01, 02, and 03 are from glacially-molded bedrock around the alpine pond at 820 m a.s.l.

#### **Bigelow Mountain, Maine**

Bigelow Mountain is a large east-west oriented ridgeline with several prominent peaks at an elevation range between 1160 m and 1260 m a.sl. in northwestern Maine. The ridgeline is composed primarily of Devonian-age pelites of varying chemical composition affected by folding in the Acadian orogeny (Osberg et al., 1985). Bigelow Mountain is characterized by steep flanks, limiting the availability of suitable boulder samples not located on steep slopes at mid-elevations. Thus, we sampled bedrock (BP-02) and a boulder (BP-03) on the ridgeline and one boulder near the base (BP-06). All boulders appear to be composed of the underlying pelitic lithology. Because we only collected three samples from Bigelow, we combine these with samples from Tumbledown Mountain (~40 km southwest) to construct a single vertical transect from northwestern Maine.

#### Jay Peak, Vermont

Jay Peak is a prominent peak at an elevation of 1210 m a.s.l. in northern Vermont surrounded primarily by low rolling hills, making it a useful sampling location to capture large-scale ice sheet thinning. Jay Peak was formed by Devonian thrust faulting, which placed a fine-grained, quartz-chlorite-albite phyllitic schist and quartzite unit (called the Jay Peak Formation)

over the predominantly graphitic schist found elsewhere in the region (Ratcliffe et al., 2011). We collected 13 samples from Jay Peak, including three from prominent quartz veins in bedrock near the exposed summit (1176 m a.s.l., JP-01 to -03) and one from a quartz vein 90 m below the summit (JP-08); all other samples are from boulders.

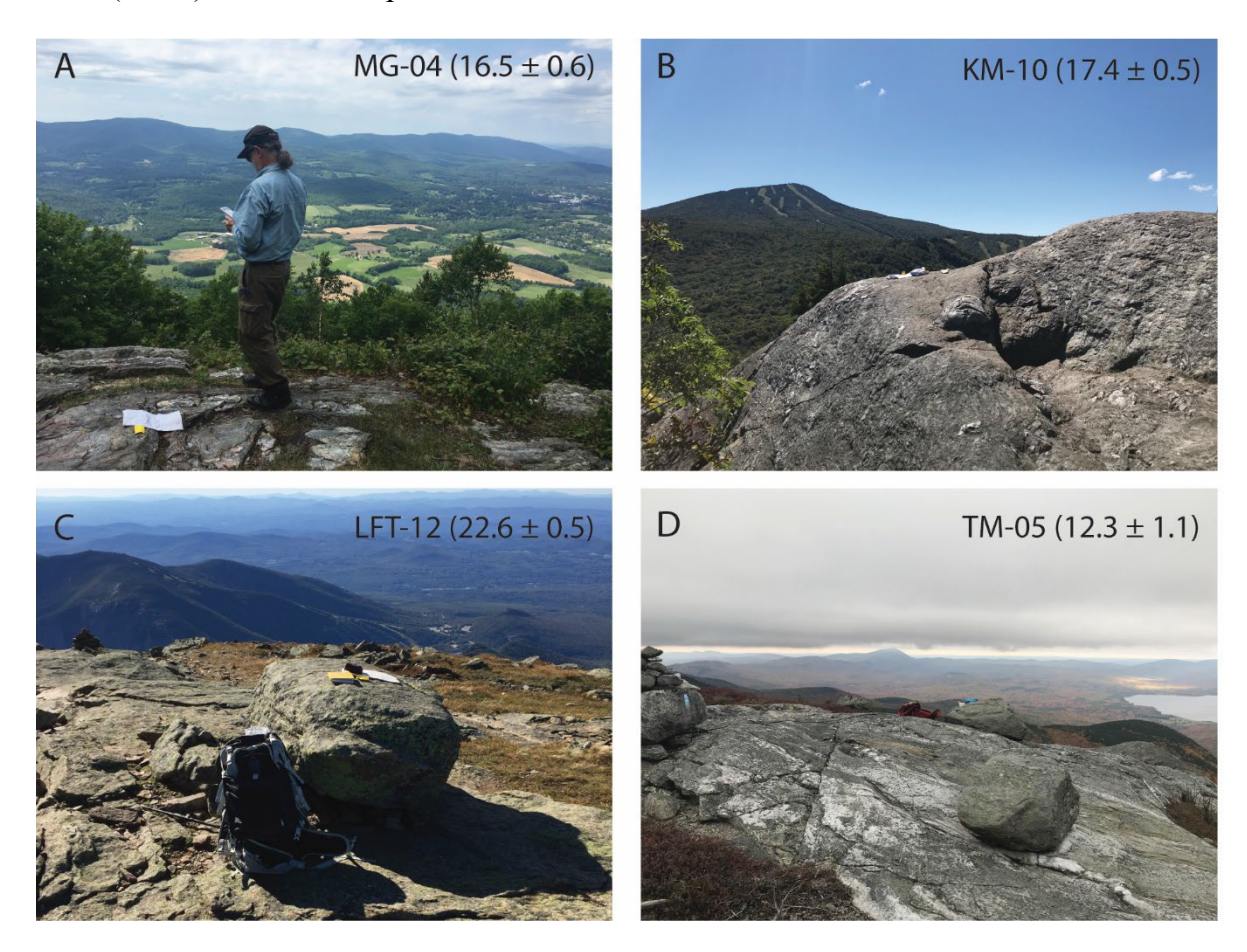


Figure 3: Example sample photos from exposure age vertical transects, including bedrock samples from Mount Greylock (A; n = 10) and Killington Peak (B; n = 12) and boulder samples from Franconia Notch (C; n = 19) and Tumbledown Mountain (D; n = 8). Labels show sample ID and exposure age  $\pm$  internal uncertainty (ka) in parentheses.

#### **RESULTS**

#### **Data Overview**

Cosmogenic nuclide exposure ages (n = 188 total, including those from previous publications) on each of 14 mountains are similar across sampled elevations, although scatter is

much more pronounced at high elevations (Fig 4; Fig 5). Exposure ages at high elevations (>1200 m a.s.l.; n = 55, including previous publications) range from 12 to 140 ka with a relative standard deviation (RSD) of 89%. Low-elevation samples (<1200 m a.s.l.; n = 133, including previous publications) are more tightly clustered, with all but three ages between 9 to 26 ka. Two young samples have ages of 1 and 5 ka, and one older sample is 52 ka. With all samples included, low-elevation samples have an RSD of 29%; RSD drops to 17% after excluding the two young and one old sample (Fig 4). We did not sample above 1200 m a.s.l. on seven mountains (Peekamoose Mt., Wachusett Mt., Mt. Greylock, Mt. Monadnock, Wachusett Mt., Tumbledown Mt., Jay Peak), their transects are thus composed entirely of low-elevation samples.

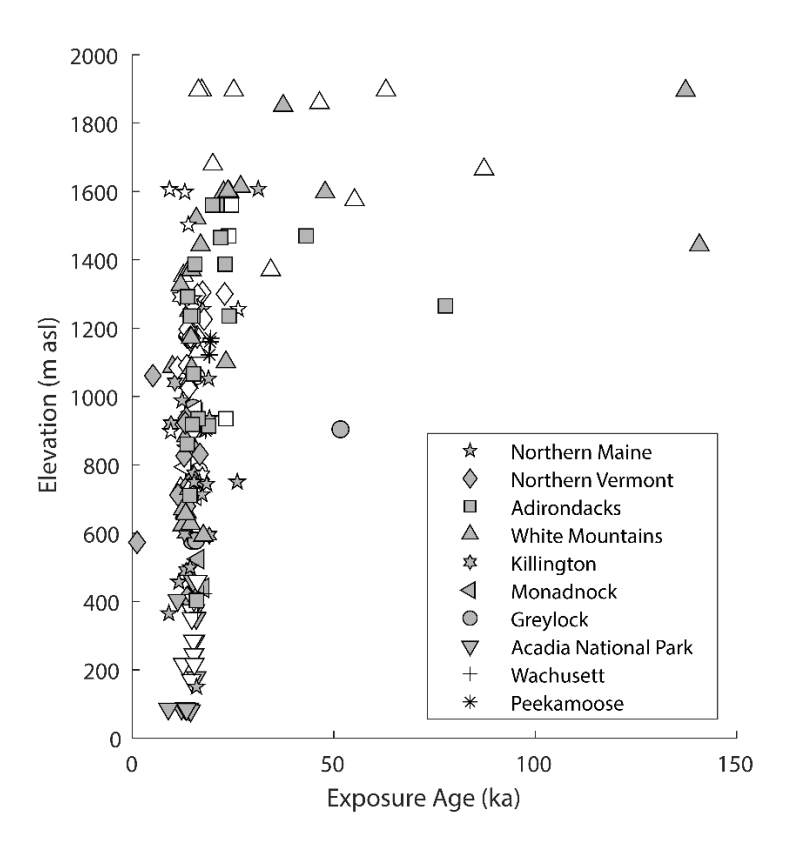


Figure 4: Exposure ages from all mountains in the northeastern U.S. plotted against elevation above sea level. Open symbols are bedrock samples, grey symbols are boulders. 'Northern Maine' includes Tumbledown Mtn., Bigelow Mtn., and Katahdin (Bierman et al., 2015; Davis et al., 2015). 'Northern

Vermont' includes Jay Peak and Mt. Mansfield (Corbett et al., 2019). 'White Mountains' includes Mt. Washington (Bierman et al., 2015; Koester et al., 2020) and Franconia Notch.

We removed 40 of the 188 samples from interpretations of LIS deglacial chronology because we believe that these samples record histories other than simple exposure since deglaciation (see GSA Data Repository). These samples have exposure ages that are either significantly younger (i.e., no age overlap considering external uncertainty; n = 22) than independent, low-elevation deglacial constraints such as calibrated glacial varves (Ridge et al., 2012) and minimum-limiting radiocarbon ages (Dalton et al., 2020), or are older than the LGM (n = 18), which we define locally as 24 ka across the study area based on the initiation of southeastern LIS retreat from the terminal moraine (Stanford et al., 2020). In both cases—ages younger than independent deglacial constraints or older than the LGM—exposure ages are unlikely to correspond to the timing of local deglaciation.

Most of the samples not included in the ice thinning analysis above 1200 m a.s.l. (n = 18) have exposure ages older than the timing of local deglaciation (n = 16), although two high-elevation samples are younger than independent, low-elevation deglacial chronologies. We infer that the older samples contain nuclides inherited from a period or periods of prior exposure, implying that glacial erosion was insufficient to remove such nuclides and agreeing with previous interpretations of old, high-elevation ages in the region (e.g., Bierman et al., 2015; Corbett et al., 2019). The two young samples at high elevations (PTMW-04, KM-02; GSA Data Repository) may have experienced post-glacial cover that partly shielded sample surfaces from cosmic radiation (Ivy-Ochs and Kober, 2008; Heyman et al., 2011).

At elevations below 1200 m a.s.l., 20 samples with ages younger than minimum-limiting deglacial chronologies and two samples with ages older than the LGM were not included in our

reconstruction of LIS deglacial chronology. The young ages reflect late-glacial or Holocene landscape processes, largely echoing earlier work on this topic (e.g., Ivy-Ochs and Kober, 2008; Heyman et al., 2011). Young boulders (e.g., JP-09, 12, KM-09, TM-08, LFT-18, BR-01; Fig 6) were likely disturbed sometime after deglaciation and thus the exposure age of their present-day upper surface corresponds to the time of disturbance. Alternatively, post-glacial cover may have caused both boulder and bedrock (e.g., TM-02, KM-02; Fig 6) ages to be younger than the timing of deglaciation (Ivy-Ochs and Kober, 2008; Heyman et al., 2011).

Where low-elevation boulder samples have ages older than other local samples (e.g., MG-07, KM-09, FW-02; Fig 6), we infer that the boulder contains nuclides inherited from prior exposure. These boulders are all composed of local bedrock lithologies and thus did not experience prolonged glacial transport and erosion. These old, low-elevation boulders may have arrived at their present locations during Holocene rockslides while retaining an inventory of inherited nuclides and/or the effects of cosmic-ray exposure initially at high elevations after the LGM (cf. Hilger et al., 2019). Exposure ages from erratic boulders (e.g., KM-11, MG-08; Fig 6) agree well with local ages, supporting previous work (e.g., Fabel et al., 2012) and suggesting erratic boulders are reasonable sampling targets in areas where bedrock has not been deeply eroded.

After identifying ages that record events other than deglaciation, remaining ages cluster tightly over hundreds of meters of elevation range at most sampling locations, with some high-and low-elevation ages from the same mountain identical within internal uncertainty (Fig 5). The similarity of ages along elevation transects suggests rapid thinning at all mountains (decimeters to meters per year). However, such statistically indistinguishable ages prevent us from constraining absolute ice thinning rates using age/elevation regressions in a Monte Carlo random

resampling framework (e.g., Johnson et al., 2014) as the range of simulated thinning rates is large and includes implausible scenarios such as ice thickening over time and thinning in excess of 10 meters per year (see GSA Data Repository).

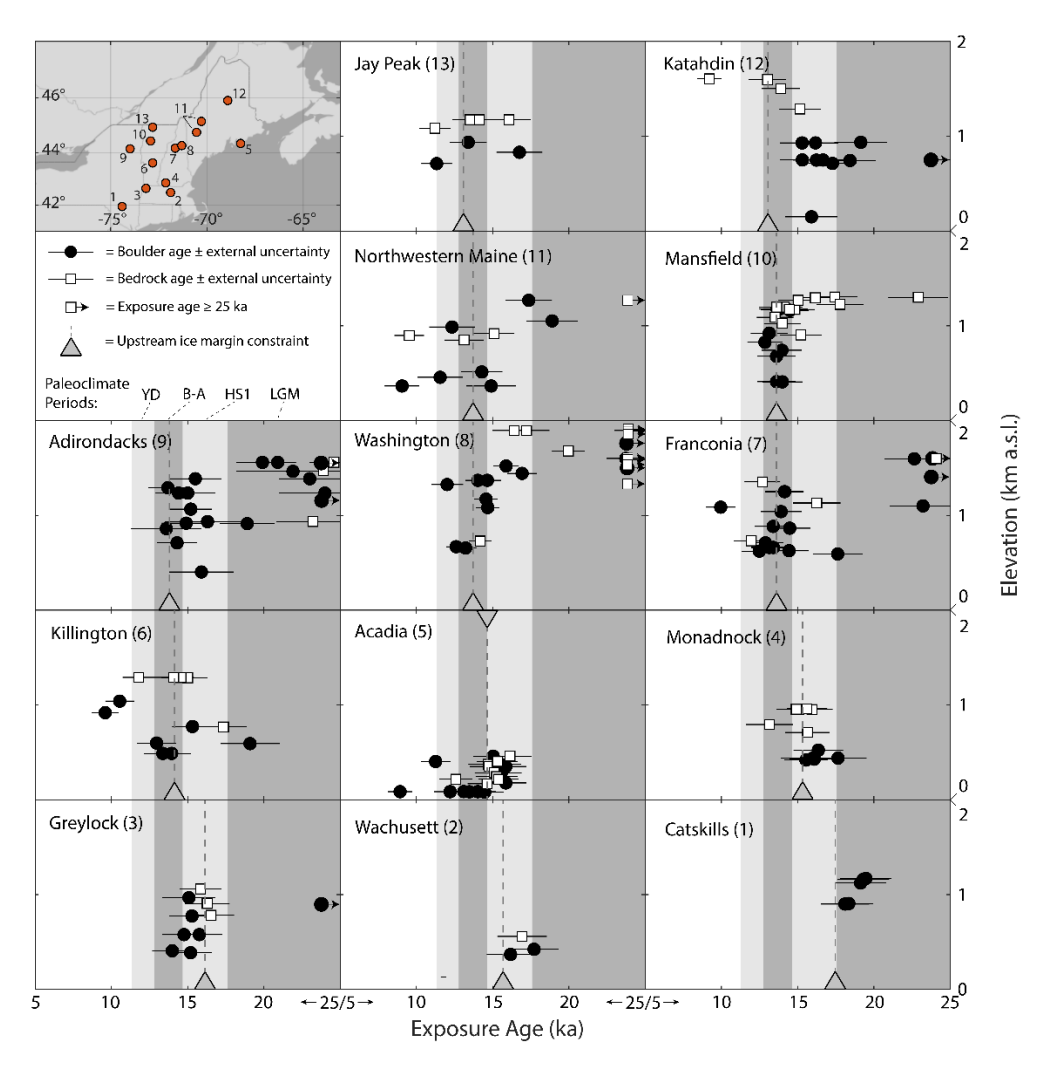


Figure 5: Exposure ages from each site plotted against elevation. Inset shows the location of each mountain, see Fig 1 for more detail. Underlying grey panels show paleoclimate periods from (Osman et al., 2021): LGM = Last Glacial Maximum, HSI = Heinrich Stadial 1, B-A = Bølling-Allerød, YD = Younger Dryas. 'Upstream ice margin constraints' are minimum limits on LIS margin positions north of (up the retreat axis from) each site and are based on the LIS reconstructions in Ridge et al. (2012) and Dalton et al. (2020).

# Peripheral vs. Up-Ice Deglaciation

431

432

433

434

435

436

437

438

439

440

441

442

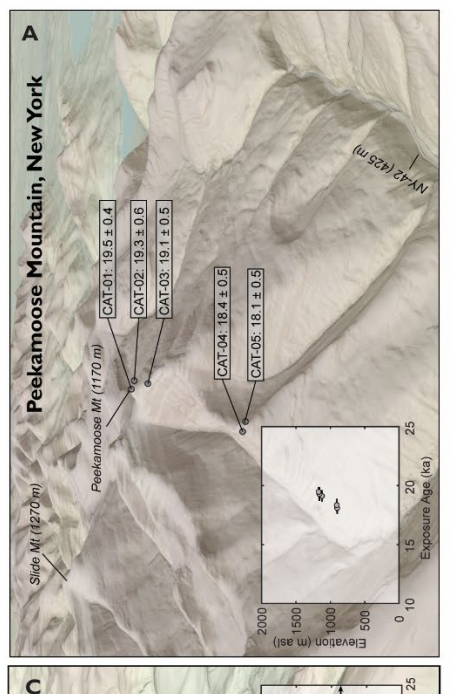
443

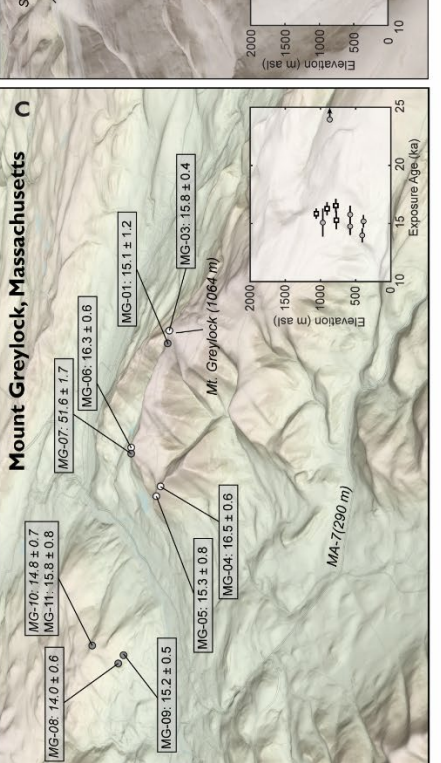
444

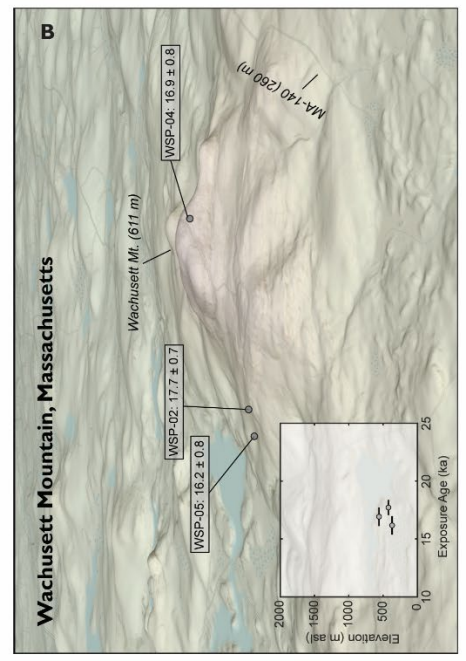
445

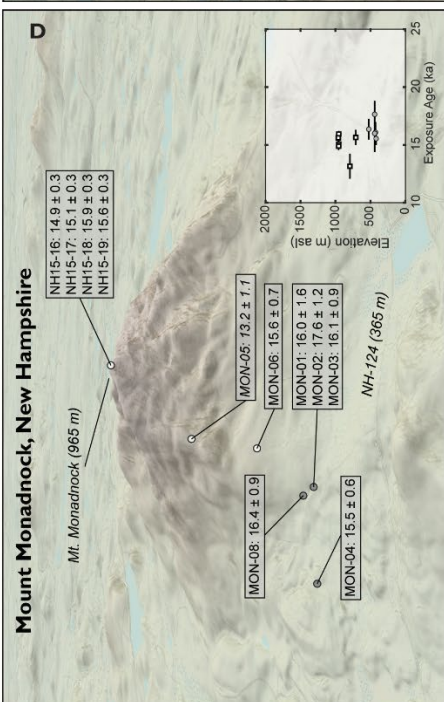
446

<sup>10</sup>Be ages differ between low-elevation (<1200 m a.s.l.) samples from 'peripheral' (transects 1 to 5 in Fig 5;  $15.9 \pm 0.3$  ka, mean  $\pm$  SE, n = 44) and 'up-ice' (transects 6 to 13 in Fig 5;  $14.9 \pm 0.2$  ka, n = 63) mountains (one way ANOVA; p = 0.004). Exposure ages from our most southerly site, Peekamoose Mountain, indicate that the LIS surface lowered below 1200 m a.s.l. in southern NY by  $18.9 \pm 1.1$  ka (n = 5; Fig 6). Exposure ages from the other four peripheral mountains are predominately from 17 to 15 ka and at Mount Greylock and Monadnock suggest ~600 m of ice thinning over this period (Fig 5, 6). As observed previously at up-ice mountains such as Mount Washington (Koester et al., 2020), Mount Mansfield (Corbett et al., 2019), and numerous sites in the Adirondack Mountains (Barth et al., 2019), our exposure ages from Franconia Notch and Killington Peak are similar across nearly 1000 m of elevation (given internal uncertainties that range from 0.4 to 0.8 kyr) and cluster between 15 and 13 ka. Exposure ages from the furthest up-ice mountains do not exhibit the same clustering between 15 and 13 ka observed at other up-ice sites. Low-elevation boulder samples from Katahdin in northern Maine have <sup>10</sup>Be ages between 18 and 15 ka (Fig 5). Bedrock and boulder <sup>10</sup>Be ages from northwestern Maine and Jay Peak, Vermont, exhibit significant scatter and range from 18 to 12 ka (Fig 5, 6).









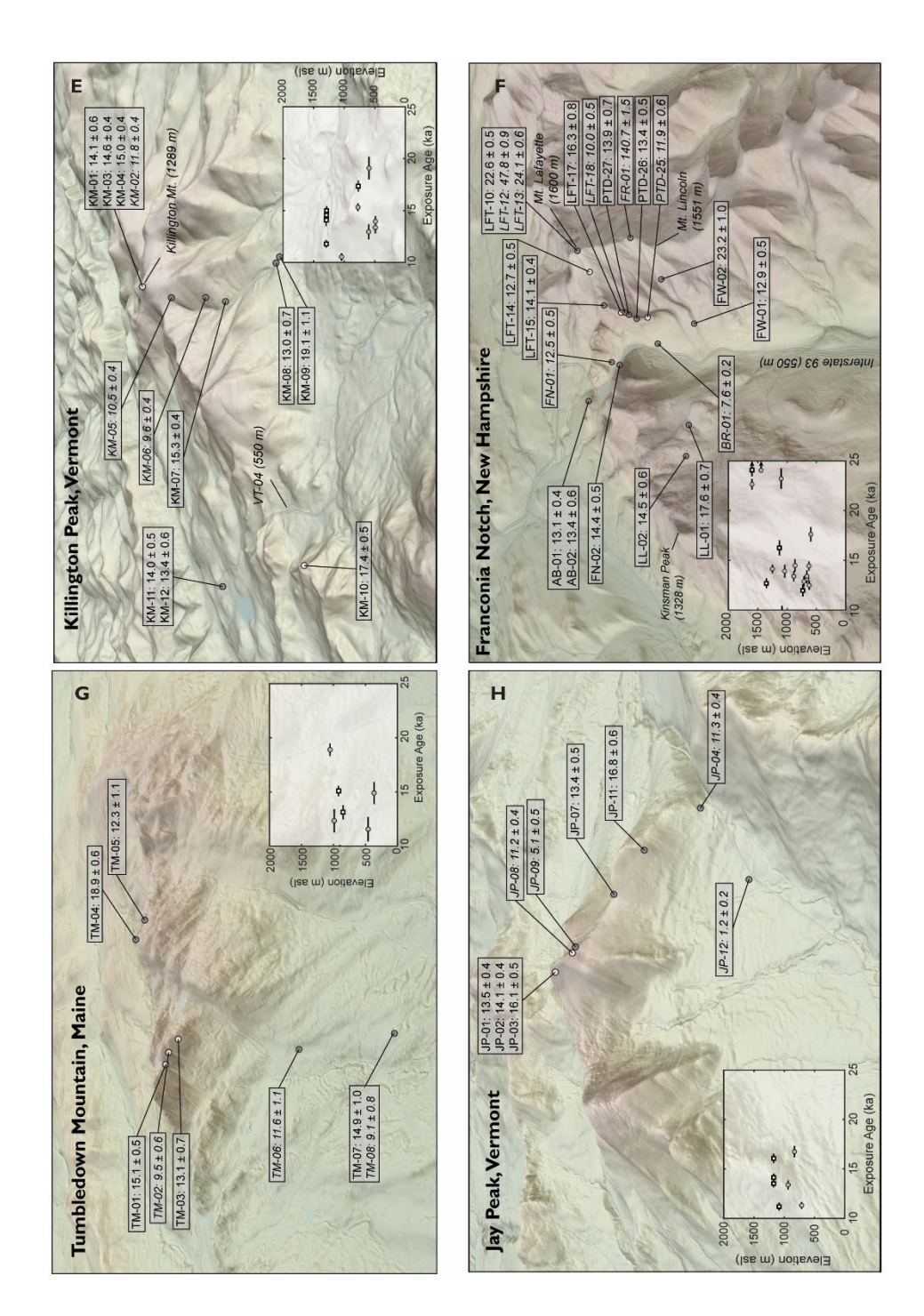


Figure 6: Oblique perspective maps showing vertical exposure age transect sites and sample locations. In each map, white circles are bedrock samples, gray circles are boulder samples, ages next to sample IDs are exposure ages and internal uncertainties (ka), and italicized samples are outliers not included in thinning reconstructions. Inset panels show exposure age vs. elevation plots for each mountain. 2D maps with spatial reference information are in the GSA Data Repository.

#### DISCUSSION

454

455

456

457

458

459

460

461

462

463

464

465

466

467

468

469

470

471

472

473

474

475

476

# Glacial and Geomorphic Implications of Exposure Ages

Our data suggest that a region-wide subglacial erosional and therefore thermal boundary typified the southeastern LIS. Such subglacial boundaries mark the transition from warm-based, deeply erosive ice at lower elevations to poly-thermal or cold-based ice of varying erosivity higher on the mountains. Tightly-clustered exposure ages consistent with the established timing of deglaciation dominate the sample population at elevations below 1200 m a.s.l.. This pattern is in stark contrast to the far more variable and older ages at high elevations on our tallest mountains. The few high-elevation ages that are similar to low-elevation ages in the same transect may have experienced deeper erosion and thus accurately record early exposure of peaks (Fig 4, 5). However, the clear presence of <sup>10</sup>Be inheritance in many high-elevation samples prevents us from confidently distinguishing between samples with and without inheritance at high elevations. Along with geomorphic evidence of minimal glacial erosion at higher elevations (e.g., Corbett et al., 2019; Koester et al., 2020), the elevation-related disparity in cosmogenic exposure ages suggests an elevation-dependent shift in the englacial thermal regime of the LIS (Sugden and Watts, 1977; Kleman and Glasser, 2007). Such subglacial erosion boundaries have been proposed for high-latitude landscapes formerly covered by LGM ice sheets, such as in Arctic Canada (Marsella et al., 2000; Marquette et al., 2004; Staiger et al., 2005; Briner et al., 2006), Scandinavia (Fabel et al., 2002; Stroeven et al., 2006; Goehring et al., 2008), Scotland (Stone et al., 1998; Stone and Ballantyne, 2006), and Greenland (Corbett et al., 2013), but, until now, the only evidence of such boundaries at midlatitudes comes from work on individual mountains in the northeastern U.S. (Bierman et al., 2015; Corbett et al., 2019; Koester et al., 2020). The exposure age compilation presented here,

which includes data from these previous regional studies, enables us to conclude that a subglacial boundary existed at approximately 1200 m a.s.l. across multiple mountain ranges in the northeastern U.S. during LIS cover.

Our exposure ages at most mountains are consistent with ice margin retreat positions as

#### Southeastern LIS Deglacial Chronology and Paleoclimate Influences

477

478

479

480

481

482

483

484

485

486

487

488

489

490

491

492

493

494

495

496

497

498

delineated by the North American Varve Chronology (NAVC; Ridge et al., 2012) and the radiocarbon-based LIS reconstruction from Dalton et al. (2020). For example, these reconstructions place the LIS margin just south of the Catskill Mountains, New York, at 18 ka, in good agreement with our exposure ages between 1200 and 900 m a.s.l. on Peekamoose Mountain  $(18.9 \pm 1.1 \text{ ka})$ . The NAVC places the LIS margin in southern New Hampshire by  $15.3 \pm 0.2$  ka (Ridge et al., 2012); our exposure ages indicate that the LIS surface lowered below 400 m a.s.l. in the same general area by 16 ka (Fig 5). The 15 to 13 ka clustering of ages at our 'up-ice' mountains correspond to accelerated ice margin retreat through northern New York, Vermont, and New Hampshire (Fig 1; Ridge et al., 2012). Ice thinning and retreat constraints together indicate that the southeastern LIS began losing mass soon after the LGM and later experienced substantial, rapid ice loss coincident with the Bølling-Allerød warm interval (B-A; ~14.6 to 12.9 ka; Osman et al., 2021; Fig 7). Exposure ages from our most southerly site, Peekamoose Mountain, yield a thinning age close to the boundary between the persistently-cold late LGM (>18 ka) and Heinrich Stadial 1 (HS1; ~18 to 14.6 ka; Osman et al., 2021; Fig 7). The early thinning indicated by these ages coincides with slow (~10 m/yr) initial retreat of the southern LIS margin from 24 to 18 ka (Ridge et al., 2012; Stanford et al., 2020). Ice thinning and retreat during the late LGM suggests that the southeastern LIS was

highly sensitive to external forcings, as the subtle rise in Northern Hemisphere insolation (Laskar et al., 2011; Fig 7) is the most plausible driver of early deglaciation (Clark et al., 2009).

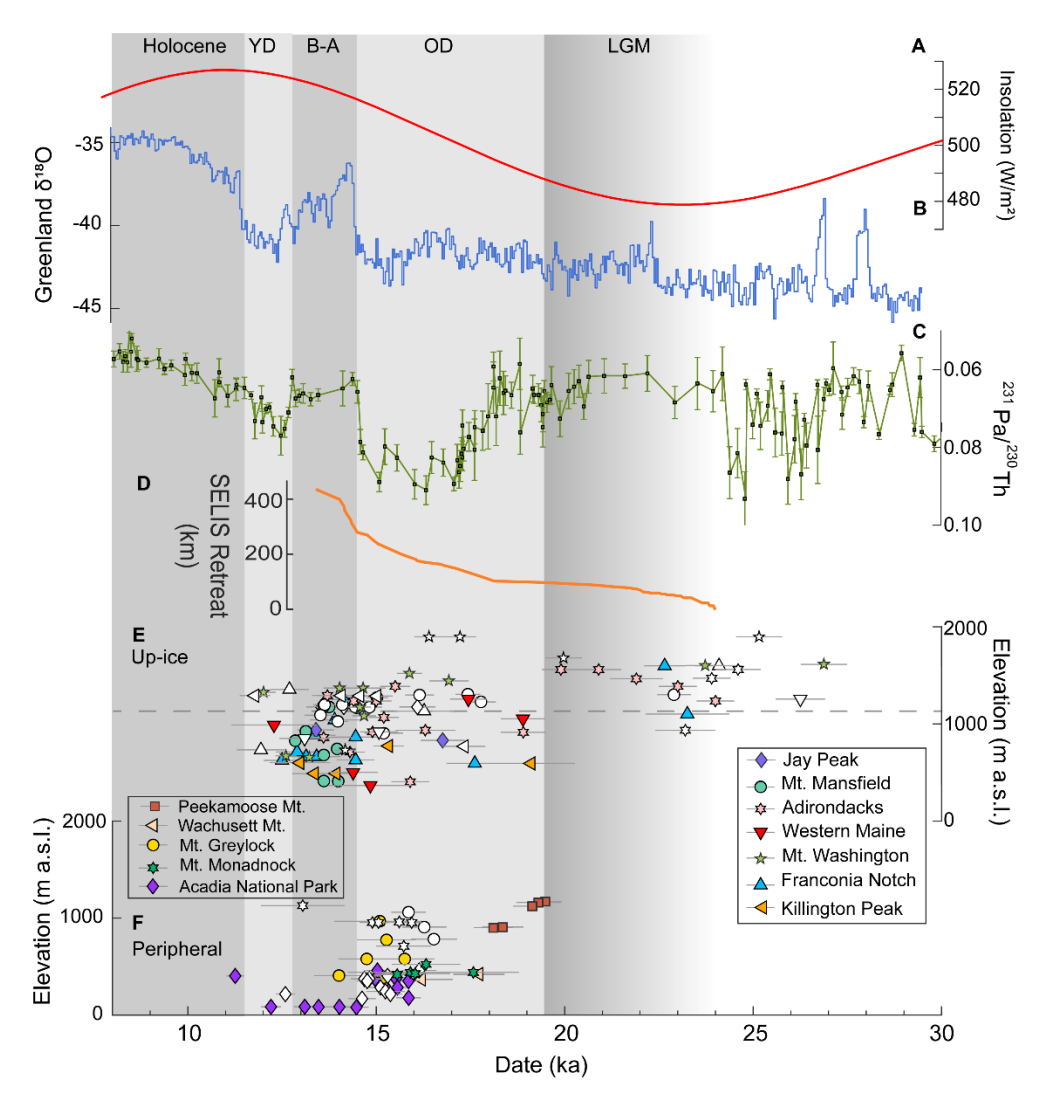


Figure 7: Southeastern LIS exposure age transects and select deglacial paleoclimate records. (A) June 21. insolation for 40°N (Laskar et al., 2011). (B) The NGRIP oxygen-isotope record (Kindler et al., 2014). (C) <sup>231</sup>Pa/<sup>230</sup>Th (a proxy for the strength of the Atlantic Meridional Overturning Circulation) record from the Bermuda Rise (Lippold et al., 2009). (D) Southeastern LIS margin retreat from varve chronologies (Ridge et al., 2012; Stanford et al., 2020) measured as km north of the Long Island terminal moraine. (E) Exposure ages from 'up-ice' transects (not including ages older than 30 ka). White symbols are bedrock samples, colored symbols are boulders. Error bars show external uncertainties on exposure ages. Dashed line shows 1200 m a.s.l. (F) Exposure ages from 'peripheral' transects. Gray boxes show established paleoclimate intervals during the deglacial period as defined by Osborne et al. (2021); OD = Oldest Dryas, B-A = Bølling-Allerød, YD = Younger Dryas.

Exposure ages from the other four peripheral mountains (dipsticks 2 to 5 in Fig 5) coincide with HS1, when Northern Hemisphere air temperatures slowly began to rise (Buizert et al., 2014; Osman et al., 2021) in response to rising atmospheric greenhouse gas concentrations (Köhler et al., 2017) and summer insolation (Laskar et al., 2011; Fig 7). These peripheral transects suggest ≥600 m of ice thinning from 17 to 15 ka and coincide with an increase in ice margin retreat speed (up to 90 m/yr) compared to earlier in the deglacial period (Ridge et al., 2012). This evidence for accelerated loss of ice during HS1 provides further evidence of a sensitive southeastern LIS. Northern Hemisphere temperature rise was only moderate during HS1 (Osman et al., 2021), although warming may have been confined mainly to summer months (Buizert et al., 2014) and therefore had immediate influence on LIS ablation rates.

Our ages and independent deglacial constraints suggest that the exposure of 'up-ice'

mountains was rapid. While our exposure ages from multiple up-ice mountains cluster between 15 and 13 ka, a moraine system north of the Franconia Notch and Mt. Washington transects is dated to approximately 14 ka (Bromley et al., 2015; Thompson et al., 2017), suggesting that, at least in northern New Hampshire, 1000 m of ice thinning occurred predominately between 15 and 14 ka. This history implies an average ice thinning rate of ~1 m/yr, agreeing with previous estimates from Koester et al. (2020) and Corbett et al. (2019) and supported by geomorphic evidence in the form of small lateral 'push' moraines interpreted as annual features recording ice thinning down some of our studied mountains (Wright, 2018).

This rapid and substantial thinning at our up-ice mountains coincided with the acceleration of ice margin retreat from 90 to 300 m/yr that is attributed to the onset of the B-A around 14.6 ka (Ridge et al., 2012). The B-A was marked by an abrupt air temperature increase around the North Atlantic that is associated with a resurgence in the strength of the Atlantic Meridional

Overturning Circulation (McManus et al., 2004; Liu et al., 2009; Fig 7). We infer that the rise in air temperatures enhanced ablation rates over the southeastern LIS, promoting accelerated ice loss. Such a scenario is supported by increased glacial varve thickness during the B-A (Ridge et al., 2012), indicative of greater summer meltwater output, and offshore sediment records that indicate a substantial increase in total LIS meltwater during the B-A (Vetter et al., 2017).

The close parallel between timing of ice margin retreat and exposure of vertical transects suggests that the southeastern LIS maintained a consistent and steep profile during deglaciation. We do not see evidence of interior thinning prior to margin retreat, as might be induced by dynamic mechanisms such as loss of buttressing ice shelves (Alvarez-Solas et al., 2013) or enhanced basal lubrication (Pfeffer et al., 2008).

# **Precision of the Dipstick Methodology**

Our exposure age/elevation transects presented here, along with previously-published transects from around the world, demonstrate that for all but the slowest thinning scenarios the dipstick approach is useful for constraining the timing of paleo-ice sheet thinning, but is unable to resolve thinning rates with precision. Most previously-published exposure age/elevation transects exhibit similar patterns to our transects, with ages that are indistinguishable within internal uncertainties (that typically range from 0.4 to 1 kyr). Such transects record thinning of the Patagonian (Boex et al., 2013), Fennoscandian (Goehring et al., 2008), Greenland (Winsor et al., 2015), and Antarctic (Johnson et al., 2014; Small et al., 2019 and references therein) Ice Sheets and span elevation ranges between 75 and 1000 m. Attempts to constrain thinning rates quantitatively from these transects produce large ranges (e.g., ~0.1 to 6 m/yr, 95% confidence interval; Johnson et al., 2014), although many of these previous studies estimate most-likely ice thinning rates around 1 m/yr (e.g., Boex et al., 2013; Johnson et al., 2014). Quantitative attempts

at constraining thinning rates produce narrow ranges only where transect ages are distinctly different with elevation (considering internal uncertainties), and thus paleo-ice thinning rates were slow. For example, a transect on Mount Hope, Antarctica, records slow ice thinning (most-likely rate = 0.17 m/yr) with a tight distribution of plausible thinning rates from Monte-Carlo analysis (0.13 to 0.24 m/yr, 95% confidence interval; Small et al., 2019).

#### **Comparisons to and Implications for Modern Ice Sheets**

Our analysis of the demise of the LIS after the LGM provides context for the current and future response of the Greenland and Antarctic Ice Sheets to climate change. Both are likely to lose substantial mass, which will result in thinning and retreat of the ice margin. Despite integrating over very different timescales, modern basin-wide thinning rates for the Greenland Ice Sheet (0.12 to 0.84 m/yr; Pritchard et al., 2009) overlap with the wide range of reconstructed paleo-ice sheet thinning rates estimated from vertical exposure age transects around the world (~0.2 to >1.5 m/yr). Thinning rates around the Antarctic Ice Sheet (~0.1 to 0.3 m/yr; Shepherd et al., 2019) are similar to reconstructed Antarctic paleo-ice-thinning rates from Small et al. (2019), especially when considering only transects with tight constraints on the range of possible rates.

Because ice sheet paleo-thinning rates based on exposure ages are time-averaged over 100's to 1000's of years, such overlaps indicate that modern rates of thinning can be sustained over centennial to millennial time scales. Most vertical exposure age transects with indistinguishable ages are inferred to represent rates of ice thinning equal to or more than 1 m/yr (Johnson et al., 2014), and therefore imply that drainage basins of the Greenland and Antarctic Ice Sheets could experience faster sustained thinning (>1 m/yr) in the future. This hypothesis is supported by extremely fast dynamic thinning rates observed in ice streams (1.5 m/yr in

Greenland, 4 to 9 m/yr in Antarctica) and the recent increase in mass loss rate from both ice sheets (Shepherd et al., 2019; The IMBIE Team, 2020).

#### **CONCLUSIONS**

We collected and processed 81 samples for cosmogenic nuclide exposure dating in the northeastern U.S. and, in conjunction with 107 previously-published exposure ages, interpret the deglacial thinning history of the southeastern LIS. Our new data support and bolster interpretations of LIS thinning history from previous publications in the region (e.g., Bierman et al., 2015; Davis et al., 2015; Koester et al., 2017, 2020; Barth et al., 2019; Corbett et al., 2019) and provide additional information about the earliest deglacial thinning. We find that the southeastern LIS began thinning very soon after the LGM, with the tops of mountains within 150 km of the margin exposed by 18 ka. Thinning continued throughout Heinrich Stadial 1 (~18 to 14.6 ka), a period characterized by slow Northern Hemisphere temperature rise, and the onset of Bølling warming at 14.6 ka is approximately coincident with rapid thinning of nearly 1000 m that we reconstruct across several mountains. Our thinning chronology matches independent ice margin retreat chronologies well, suggesting that the southeastern LIS margin retained a consistent and steep profile as it retreated through the northeastern United States.

Our data also support suggestions from previous work that an englacial thermal boundary in the LIS caused the magnitude of glacial erosion to differ above and below ~1200 m a.s.l.. Warm-based ice caused substantial erosion at lower elevations and cosmogenic measurements yield mostly deglacial ages. Above ~1200 m a.s.l., subglacial erosion was minimal and spatially heterogeneous, as indicated by variable and older exposure ages that likely contain nuclides inherited from pre-LGM exposure and record processes other than simple exposure.

The thinning chronology we reconstruct here echoes chronologies from other paleo-ice sheets, which imply ice sheet thinning rates exceeding drainage-basin-wide ice thinning rates observed so far on modern ice sheets. Our conclusion, that LIS thinning and retreat accelerated due to North Atlantic warming during the B-A, supports the sobering possibility of fast and sustained ice loss from ice sheets in the future as climate warms.

#### REFERENCES CITED

608

626

627

628

629 630

631

632

633

634

635

636

637

638

639

640

641

642

- Abe-Ouchi, A., Saito, F., Kageyama, M., Braconnot, P., Harrison, S. P., Lambeck, K., Otto Bliesner, B. L., Peltier, W. R., Tarasov, L., Peterschmitt, J. Y., and Takahashi, K., 2015,
   Ice-sheet configuration in the CMIP5/PMIP3 Last Glacial Maximum experiments:
   Geoscientific Model Development, v. 8, no. 11, p. 3621-3637.
- Allen, T., Creasy, J., Davis, P. T., Eusden, J. D., Fowler, B., and Thompson, W. B., The Notches:
   Bedrock and Surficial Geology of New Hampshire's White Mountains, *in* Proceedings
   Guidebook of Field Trips for the Geological Society of America's 2001 Annual Meeting,
   Boston, 2001, Geological Society of America, Boulder, Colorado, p. C1-C33.
- 617 Alvarez-Solas, J., Robinson, A., Montoya, M., and Ritz, C., 2013, Iceberg discharges of the last 618 glacial period driven by oceanic circulation changes: Proc Natl Acad Sci U S A, v. 110, 619 no. 41, p. 16350-16354.
- Balco, G., 2011, Contributions and unrealized potential contributions of cosmogenic-nuclide exposure dating to glacier chronology, 1990–2010: Quaternary Science Reviews, v. 30, no. 1-2, p. 3-27.
- Balco, G., Briner, J., Finkel, R. C., Rayburn, J. A., Ridge, J. C., and Schaefer, J. M., 2009,
   Regional beryllium-10 production rate calibration for late-glacial northeastern North
   America: Quaternary Geochronology, v. 4, no. 2, p. 93-107.
  - Balco, G., and Schaefer, J., 2006, Cosmogenic-nuclide and varve chronologies for the deglaciation of southern New England: Quaternary Geochronology, v. 1, no. 1, p. 15-28.
  - Balco, G., Stone, J. O., Lifton, N. A., and Dunai, T. J., 2008, A complete and easily accessible means of calculating surface exposure ages or erosion rates from <sup>10</sup>Be and <sup>26</sup>Al measurements: Quaternary Geochronology, v. 3, no. 3, p. 174-195.
  - Barth, A. M., Marcott, S. A., Licciardi, J. M., and Shakun, J. D., 2019, Deglacial thinning of the Laurentide Ice Sheet in the Adirondack Mountains, New York, USA, revealed by <sup>36</sup>Cl exposure dating: Paleoceanography and Paleoclimatology, v. 34, no. 6, p. 946-953.
  - Bierman, P., Marsella, K., Patterson, C., Davis, P. T., and Caffee, M., 1999, Mid-Pleistocene cosmogenic minimum-age limits for pre-Wisconsinan glacial surfaces in southwestern Minnesorta and southern Baffin Island: a multiple nuclide approach: Geomorphology, v. 27, no. 1-2, p. 25-39.
  - Bierman, P. R., Davis, P. T., Corbett, L. B., Lifton, N. A., and Finkel, R. C., 2015, Cold-based Laurentide ice covered New England's highest summits during the Last Glacial Maximum: Geology, v. 43, p. 1059-1062.
  - Boex, J., Fogwill, C., Harrison, S., Glasser, N. F., Hein, A., Schnabel, C., and Xu, S., 2013, Rapid thinning of the late Pleistocene Patagonian Ice Sheet followed migration of the Southern Westerlies: Scientific Reports, v. 3, no. 1.
- Briner, J. P., Miller, G. H., Davis, P. T., and Finkel, R. C., 2005, Cosmogenic exposure dating in arctic glacial landscapes: implications for the glacial history of northeastern Baffin Island, Arctic Canada: Canadian Journal of Earth Sciences, v. 42, no. 1, p. 67-84.
- Briner, J. P., Miller, G. H., Davis, P. T., and Finkel, R. C., 2006, Cosmogenic radionuclides from fiord landscapes support differential erosion by overriding ice sheets: Geological Society of America Bulletin, v. 118, no. 3-4, p. 406-420.

- Bromley, G. R. M., Hall, B. L., Thompson, W. B., Kaplan, M. R., Garcia, J. L., and Schaefer, J.
   M., 2015, Late glacial fluctuations of the Laurentide Ice Sheet in the White Mountains of
   Maine and New Hampshire, U.S.A.: Quaternary Research, v. 83, no. 3, p. 522-530.
- Bromley, G. R. M., Hall, B. L., Thompson, W. B., and Lowell, T. V., 2019, Age of the Berlin moraine complex, New Hampshire, USA, and implications for ice sheet dynamics and climate during Termination 1: Quaternary Research, v. 94, p. 80-93.

657

658

659

660

661

662

663

664

665

666

670

671

672

682

683

684

- Brook, E. J., Nesje, A., Lehman, S. J., Raisbeck, G. M., and Yiou, F., 1996, Cosmogenic nuclide exposure ages along a vertical transect in western Norway: Implications for the height of the Fennoscandian ice sheet: Geology, v. 24, no. 3, p. 207-210.
- Buizert, C., Gkinis, V., Severinghaus, J. P., He, F., Lecavalier, B. S., Kindler, P., Leuenberger, M., Carlson, A. E., Vinther, B., Masson-Delmotte, V., White, J. W., Liu, Z., Otto-Bliesner, B., and Brook, E. J., 2014, Greenland temperature response to climate forcing during the last deglaciation: Science, v. 345, no. 6201, p. 1177-1180.
- Clark, C. D., Ely, J. C., Greenwood, S. L., Hughes, A. L. C., Meehan, R., Barr, I. D., Bateman, M. D., Bradwell, T., Doole, J., Evans, D. J. A., Jordan, C. J., Monteys, X., Pellicer, X. M., and Sheehy, M., 2018, BRITICE Glacial Map, version 2: a map and GIS database of glacial landforms of the last British-Irish Ice Sheet: Boreas, v. 47, no. 1, p. 11-e18.
- Clark, P. U., Dyke, A. S., Shakun, J. D., Carlson, A. E., Clark, J., Wohlfarth, B., Mitrovica, J. X.,
  Hostetler, S. W., and McCabe, A. M., 2009, The Last Glacial Maximum: Science, v. 325,
  no. 5941, p. 710-714.
  - Clark, P. U., Marshall, S. J., Clarke, G. K., Hostetler, S. W., Licciardi, J. M., and Teller, J. T., 2001, Freshwater forcing of abrupt climate change during the last glaciation: Science, v. 293, no. 5528, p. 283-287.
- Clark, P. U., Shakun, J. D., Baker, P. A., Bartlein, P. J., Brewer, S., Brook, E., Carlson, A. E.,
  Cheng, H., Kaufman, D. S., Liu, Z., Marchitto, T. M., Mix, A. C., Morrill, C., OttoBliesner, B. L., Pahnke, K., Russell, J. M., Whitlock, C., Adkins, J. F., Blois, J. L., Clark,
  J., Colman, S. M., Curry, W. B., Flower, B. P., He, F., Johnson, T. C., Lynch-Stieglitz, J.,
  Markgraf, V., McManus, J., Mitrovica, J. X., Moreno, P. I., and Williams, J. W., 2012,
  Global climate evolution during the last deglaciation: Proc Natl Acad Sci U S A, v. 109,
  no. 19, p. E1134-1142.
- 680 Clark, P. U., and Tarasov, L., 2014, Closing the sea level budget at the Last Glacial Maximum: 681 Proceedings of the National Academy of Sciences, v. 111, no. 45, p. 15861-15862.
  - Corbett, L. B., Bierman, P. R., Graly, J. A., Neumann, T. A., and Rood, D. H., 2013, Constraining landscape history and glacial erosivity using paired cosmogenic nuclides in Upernavik, northwest Greenland: Geological Society of America Bulletin, v. 125, no. 9-10, p. 1539-1553.
- 686 Corbett, L. B., Bierman, P. R., and Rood, D. H., 2016, An approach for optimizing in situ cosmogenic <sup>10</sup>Be sample preparation: Quaternary Geochronology, v. 33, p. 24-34.
- 688 Corbett, L. B., Bierman, P. R., Woodruff, T. E., and Caffee, M. W., 2019a, A homogeneous 689 liquid reference material for monitoring the quality and reproducibility of in situ 690 cosmogenic <sup>10</sup>Be and <sup>26</sup>Al analyses: Nuclear Instruments and Methods in Physics 691 Research Section B: Beam Interactions with Materials and Atoms, v. 456, p. 180-185.
- Corbett, L. B., Bierman, P. R., Wright, S. F., Shakun, J. D., Davis, P. T., Goehring, B. M.,
   Halsted, C. T., Koester, A. J., Caffee, M. W., and Zimmerman, S. R., 2019b, Analysis of

- multiple cosmogenic nuclides constrains Laurentide Ice Sheet history and process on Mt. Mansfield, Vermont's highest peak: Quaternary Science Reviews, v. 205, p. 234-246.
- Dalton, A. S., Margold, M., Stokes, C. R., Tarasov, L., Dyke, A. S., Adams, R. S., Allard, S.,
  Arends, H. E., Atkinson, N., Attig, J. W., Barnett, P. J., Barnett, R. L., Batterson, M.,
  Bernatchez, P., Borns, H. W., Breckenridge, A., Briner, J. P., Brouard, E., Campbell, J.
  E., Carlson, A. E., Clague, J. J., Curry, B. B., Daigneault, R.-A., Dubé-Loubert, H.,
- Easterbrook, D. J., Franzi, D. A., Friedrich, H. G., Funder, S., Gauthier, M. S., Gowan, A. S., Harris, K. L., Hétu, B., Hooyer, T. S., Jennings, C. E., Johnson, M. D., Kehew, A. E.,
- Kelley, S. E., Kerr, D., King, E. L., Kjeldsen, K. K., Knaeble, A. R., Lajeunesse, P.,
- Lakeman, T. R., Lamothe, M., Larson, P., Lavoie, M., Loope, H. M., Lowell, T. V.,
- Lusardi, B. A., Manz, L., McMartin, I., Nixon, F. C., Occhietti, S., Parkhill, M. A., Piper, D. J. W., Pronk, A. G., Richard, P. J. H., Ridge, J. C., Ross, M., Roy, M., Seaman, A.,
- Shaw, J., Stea, R. R., Teller, J. T., Thompson, W. B., Thorleifson, L. H., Utting, D. J.,
- Veillette, J. J., Ward, B. C., Weddle, T. K., and Wright, H. E., 2020, An updated radiocarbon-based ice margin chronology for the last deglaciation of the North American

712

713

714

715

716

717

718

719

720 721

722

723

724

725

726 727

728

729

730

731

- radiocarbon-based ice margin chronology for the last deglaciation of the North American
   Ice Sheet Complex: Quaternary Science Reviews, v. 234.
   Davis, P. T., 1989, Late Quaternary glacial history of Mt. Katahdin and the nunatak hypothesis:
  - Davis, P. T., 1989, Late Quaternary glacial history of Mt. Katahdin and the nunatak hypothesis: Maine Geological Survey: Studies in Maine Geology, v. 6, p. 119-134.
  - Davis, P. T., Bierman, P. R., Corbett, L. B., and Finkel, R. C., 2015, Cosmogenic exposure age evidence for rapid Laurentide deglaciation of the Katahdin area, west-central Maine, USA, 16 to 15 ka: Quaternary Science Reviews, v. 116, p. 95-105.
  - Fabel, D., Ballantyne, C. K., and Xu, S., 2012, Trimlines, blockfields, mountain-top erratics and the vertical dimensions of the last British–Irish Ice Sheet in NW Scotland: Quaternary Science Reviews, v. 55, p. 91-102.
  - Fabel, D., Stroeven, A. P., Harbor, J., Kleman, J., Elmore, D., and Fink, D., 2002, Landscape preservation under Fennoscandian ice sheets determined from in situ produced <sup>10</sup>Be and <sup>26</sup>Al: Earth and Planetary Science Letters, v. 201, no. 2, p. 397-406.
  - Goehring, B. M., Brook, E. J., Linge, H., Raisbeck, G. M., and Yiou, F., 2008, Beryllium-10 exposure ages of erratic boulders in southern Norway and implications for the history of the Fennoscandian Ice Sheet: Quaternary Science Reviews, v. 27, no. 3-4, p. 320-336.
  - Gowan, E. J., Zhang, X., Khosravi, S., Rovere, A., Stocchi, P., Hughes, A. L. C., Gyllencreutz, R., Mangerud, J., Svendsen, J. I., and Lohmann, G., 2021, A new global ice sheet reconstruction for the past 80 000 years: Nat Commun, v. 12, no. 1, p. 1199.
  - Gregoire, L. J., Payne, A. J., and Valdes, P. J., 2012, Deglacial rapid sea level rises caused by ice-sheet saddle collapses: Nature, v. 487, no. 7406, p. 219-222.
  - Halsted, C. T., Bierman, P. R., Corbett, L. B., Shakun, J. D., Davis, P. T., and Caffee, M. W., 2021, Inaccuracies in deglacial chronometers recording Laurentide Ice Sheet retreat in the northeastern United States: presence, magnitude, and controls, *in* Proceedings Geological Society of America Annual Meeting, Portland, OR, Volume 53, Abstracts with Programs.
- Heyman, J., Applegate, P. J., Blomdin, R., Gribenski, N., Harbor, J. M., and Stroeven, A. P.,
   2016, Boulder height exposure age relationships from a global glacial <sup>10</sup>Be compilation:
   Quaternary Geochronology, v. 34, p. 1-11.
- Heyman, J., Stroeven, A. P., Harbor, J. M., and Caffee, M. W., 2011, Too young or too old: Evaluating cosmogenic exposure dating based on an analysis of compiled boulder exposure ages: Earth and Planetary Science Letters, v. 302, no. 1-2, p. 71-80.

- Hilger, P., Gosse, J. C., and Hermanns, R. L., 2019, How significant is inheritance when dating rockslide boulders with terrestrial cosmogenic nuclide dating?—a case study of an historic event: Landslides, v. 16, no. 4, p. 729-738.
- Hodgdon, T.S., 2016, Developing a chronology for thinning of the Laurentide Ice Sheet in New Hampshire during the last deglaciation: M.S. thesis, University of New Hampshire, 46 p.
  - Ivy-Ochs, S., and Kober, F., 2008, Surface exposure dating with cosmogenic nuclides: Quaternary Science Journal, v. 57, no. 1/2, p. 179-209.

- Ivy-Ochs, S., Schluchter, C., Kubik, P., Dittrich-Hannen, B., and Beer, J., 1995, Minimum <sup>10</sup>Be exposure ages of early Pliocene for the Table Mountain Plateau and the Sirius Group at Mount Fleming, Dry Valleys, Antarctica: Geology, v. 23, no. 11, p. 1007-1010.
- Johnson, J. S., Bentley, M. J., Smith, J. A., Finkel, R. C., Rood, D. H., Gohl, K., Balco, G., Larter, R. D., and Schaefer, J. M., 2014, Rapid thinning of Pine Island Glacier in the early Holocene: Science, v. 343, no. 6174, p. 999-1001.
- Kindler, P., Guillevic, M., Baumgartner, M., Schwander, J., Landais, A., Leuenberger, M., 2014. Temperature reconstruction from 10 to 120 kyr b2k from the NGRIP ice core: Climate of the Past, v. 10, no. 2, p. 887–902.
- Kleman, J., and Glasser, N. F., 2007, The subglacial thermal organisation (STO) of ice sheets: Quaternary Science Reviews, v. 26, no. 5-6, p. 585-597.
- Koester, A. J., Shakun, J. D., Bierman, P. R., Davis, P. T., Corbett, L. B., Braun, D., and Zimmerman, S. R., 2017, Rapid thinning of the Laurentide Ice Sheet in coastal Maine, USA, during late Heinrich Stadial 1: Quaternary Science Reviews, v. 163, p. 180-192.
- Koester, A. J., Shakun, J. D., Bierman, P. R., Davis, P. T., Corbett, L. B., Goehring, B. M., Vickers, A. C., and Zimmerman, S. R., 2020, Laurentide ice sheet thinning and erosive regimes at Mount Washington, New Hampshire, inferred from multiple cosmogenic nuclides, *in* Waitt, R. B., Thackray, G. D., and Gillespie, A. R., eds., Untangling the Quaternary Period—A Legacy of Stephen C. Porter, Geological Society of America Special Paper 548: Boulder, Colorado, p. 299-314.
- Kohl, C. P., and Nishiizumi, K., 1992, Chemical isolation of quartz for measurement of in-situ produced cosmogenic nuclides: Geochimica et Cosmochimica Acta, v. 56, no. 9, p. 3583-3587.
- Köhler, P., Nehrbass-Ahles, C., Schmitt, J., Stocker, T. F., and Fischer, H., 2017, A 156 kyr smoothed history of the atmospheric greenhouse gases CO<sub>2</sub>, CH<sub>4</sub>, and N<sub>2</sub>O and their radiative forcing: Earth System Science Data, v. 9, no. 1, p. 363-387.
- Lambeck, K., Purcell, A., and Zhao, S., 2017, The North American Late Wisconsin ice sheet and mantle viscosity from glacial rebound analyses: Quaternary Science Reviews, v. 158, p. 172-210.
- Lambeck, K., Rouby, H., Purcell, A., Sun, Y., and Sambridge, M., 2014, Sea level and global ice
   volumes from the Last Glacial Maximum to the Holocene: Proc Natl Acad Sci U S A, v.
   111, no. 43, p. 15296-15303.
- Laskar, J., Fienga, A., Gastineau, M., and Manche, H., 2011, La2010: a new orbital solution for the long-term motion of the Earth: Astronomy & Astrophysics, v. 532, n. A89.
- Lifton, N., Sato, T., and Dunai, T. J., 2014, Scaling in situ cosmogenic nuclide production rates using analytical approximations to atmospheric cosmic-ray fluxes: Earth and Planetary Science Letters, v. 386, p. 149-160.

- Lin, Y., Hibbert, F. D., Whitehouse, P. L., Woodroffe, S. A., Purcell, A., Shennan, I., and
   Bradley, S. L., 2021, A reconciled solution of Meltwater Pulse 1A sources using sea-level
   fingerprinting: Nat Commun, v. 12, no. 1, p. 2015.
- Lippold, J., Grutzner, J., Winter, D., Lahaye, Y., Mangini, A., and Christl, M., 2009, Does sedimentary <sup>231</sup>Pa/<sup>230Th</sup> from the Bermuda Rise monitor past Atlantic meridional overturning circulation?: Geophysical Research Letters, v. 36, n. 12.

790

791

792

793

794

795

796

797

798 799

800

801

802

803

804 805

806

807

808

- Liu, Z., Otto-Bliesner, B. L., He, F., Brady, E. C., Tomas, R., Clark, P. U., Carlson, A. E., Lynch-Stieglitz, J., Curry, W., Brook, E., Erickson, D., Jacob, R., Kutzbach, J., and Cheng, J., 2009, Transient simulation of last deglaciation with a new mechanism for Bolling-Allerod warming: Science, v. 325, no. 5938, p. 310-314.
- Lyons, J. B., Bothner, W. A., Moench, R. H., and Thompson Jr., J. B., 1997, Bedrock geologic map of New Hampshire: United States Geological Survey, scale 1:250,000.
- Mackintosh, A., White, D., Fink, D., Gore, D. B., Pickard, J., and Fanning, P. C., 2007, Exposure ages from mountain dipsticks in Mac. Robertson Land, East Antarctica, indicate little change in ice-sheet thickness since the Last Glacial Maximum: Geology, v. 35, no. 6, p. 551.
- Marquette, G. C., Gray, J. T., Gosse, J. C., Courchesne, F., Stockli, L., Macpherson, G., and Finkel, R., 2004, Felsenmeer persistence under non-erosive ice in the Torngat and Kaumajet mountains, Quebec and Labrador, as determined by soil weathering and cosmogenic nuclide exposure dating: Canadian Journal of Earth Sciences, v. 41, no. 1, p. 19-38.
- Marsella, K. A., Bierman, P. R., Davis, P. T., and Caffee, M. W., 2000, Cosmogenic <sup>10</sup>Be and <sup>26</sup>Al ages for the Last Glacial Maximum, eastern Baffin Island, Arctic Canada: Geological Society of America Bulletin, v. 112, no. 7, p. 1296-1312.
- McManus, J. F., Francois, R., Gherardi, J. M., Keigwin, L. D., and Brown-Leger, S., 2004, Collapse and rapid resumption of Atlantic meridional circulation linked to deglacial climate changes: Nature, v. 428, no. 6985, p. 834-837.
- Moench, R. H., and Pankiwskyj, K. A., 1988, Geologic map of western interior Maine: United States Geological Survey and Maine Geological Survey, scale 1:250,000.
- Nishiizumi, K., Imamura, M., Caffee, M. W., Southon, J. R., Finkel, R. C., and McAninch, J., 2007, Absolute calibration of <sup>10</sup>Be AMS standards: Nuclear Instruments and Methods in Physics Research Section B: Beam Interactions with Materials and Atoms, v. 258, no. 2, p. 403-413.
- Nishiizumi, K., Kohl, C. P., Arnold, J. R., Klein, J., Fink, D., and Middleton, R., 1991, Cosmic ray produced <sup>10</sup>Be and <sup>26</sup>Al in Antarctic rocks: exposure and erosion history: Earth and Planetary Science Letters, v. 104, no. 2-4, p. 440-454.
- Nishiizumi, K., Winterer, E.L., Kohl, C.P., Klein, J., Middleton, R., Lal, D., and Arnold, J.R., 1989, Cosmic ray production rates of <sup>10</sup>Be and <sup>26</sup>Al in quartz from glacially polished rocks: Journal of Geophysical Research: Solid Earth, v. 94, n. B12, p. 17907-17915.
- Osberg, P. H., Hussey, A. M., and Boone, G. M., 1985, Bedrock geologic map of Maine: Maine Geological Survey, scale 1:500,000.
- Osman, M. B., Tierney, J. E., Zhu, J., Tardif, R., Hakim, G. J., King, J., and Poulsen, C. J., 2021, Globally resolved surface temperatures since the Last Glacial Maximum: Nature, v. 599, no. 7884, p. 239-244.

- Peltier, W. R., Argus, D. F., and Drummond, R., 2015, Space geodesy constrains ice age terminal deglaciation: The global ICE-6G\_C (VM5a) model: Journal of Geophysical Research: Solid Earth, v. 120, no. 1, p. 450-487.
- Peteet, D. M., Beh, M., Orr, C., Kurdyla, D., Nichols, J., and Guilderson, T., 2012, Delayed deglaciation or extreme Arctic conditions 21-16 cal. kyr at southeastern Laurentide Ice Sheet margin?: Geophysical Research Letters, v. 39, no. 11, p. n/a-n/a.

- Pfeffer, W. T., Harper, J. T., and O'Neel, S., 2008, Kinematic constraints on glacier contributions to 21st-century sea-level rise: Science, v. 321, no. 5894, p. 1340-1343.
  - Phillips, F. M., Zreda, M. G., Smith, S. S., Elmore, D., Kubik, P., and Sharma, P., 1990, Cosmogenic Chlorine-36 chronology for glacial deposits at Bloody Canyon, eastern Sierra Nevada: Science, v. 248, no. 4962, p. 1529-1532.
  - Pritchard, H. D., Arthern, R. J., Vaughan, D. G., and Edwards, L. A., 2009, Extensive dynamic thinning on the margins of the Greenland and Antarctic ice sheets: Nature, v. 461, no. 7266, p. 971-975.
  - Ratcliffe, N. M., Stanley, R. S., and Potter, D. B., 1993, Bedrock geologic map of the Williamstown and North Adams quadrangles, Massachusetts and Vermont, and part of the Cheshire quadrangle, Massachusetts: United States Geological Survey, Massachusetts Department of Public Works, and the Vermont Geological Survey, scale 1:24,000.
  - Ratcliffe, N. M., Walsh, G. J., Gale, M. H., Masonic, L. M., and Estabrook, J. R., 2011, Bedrock geologic map of Vermont: United States Geological Survey, Vermont Agency of Natural Resources, and the Vermont Geological Survey, scale 1:100,000.
  - Ridge, J. C., Balco, G., Bayless, R. L., Beck, C. C., Carter, L. B., Dean, J. L., Voytek, E. B., and Wei, J. H., 2012, The new North American Varve Chronology: A precise record of southeastern Laurentide Ice Sheet deglaciation and climate, 18.2-12.5 kyr BP, and correlations with Greenland ice core records: American Journal of Science, v. 312, no. 7, p. 685-722.
  - Schildgen, T. F., Phillips, W. M., and Purves, R. S., 2005, Simulation of snow shielding corrections for cosmogenic nuclide surface exposure studies: Geomorphology, v. 64, no. 1-2, p. 67-85.
  - Shepherd, A., Gilbert, L., Muir, A. S., Konrad, H., McMillan, M., Slater, T., Briggs, K. H., Sundal, A. V., Hogg, A. E., and Engdahl, M. E., 2019, Trends in Antarctic Ice Sheet Elevation and Mass: Geophysical Research Letters, v. 46, no. 14, p. 8174-8183.
  - Sirkin, L. A., and Stuckenrath, R., 1980, The Portwashingtonian warm interval in the northern Atlantic coastal plain: Geological Society of America Bulletin, v. 91, no. 6, p. 332-336.
  - Small, D., Bentley, M. J., Jones, R. S., Pittard, M. L., and Whitehouse, P. L., 2019, Antarctic ice sheet palaeo-thinning rates from vertical transects of cosmogenic exposure ages: Quaternary Science Reviews, v. 206, p. 65-80.
  - Staiger, J. K. W., Gosse, J. C., Johnson, J. V., Fastook, J., Gray, J. T., Stockli, D. F., Stockli, L., and Finkel, R., 2005, Quaternary relief generation by polythermal glacier ice: Earth Surface Processes and Landforms, v. 30, no. 9, p. 1145-1159.
- Stanford, S. D., Stone, B., Ridge, J. C., Witte, R. W., Pardi, R., and Reimer, G. E., 2020, Chronology of Laurentide glaciation in New Jersey and the New York City area, United States: Quaternary Research, v. 99, p. 142-167.

- Steig, E. J., Wolfe, A. P., and Miller, G. H., 1998, Wisconsinan refugia and the glacial history of eastern Baffin Island, Arctic Canada: Coupled evidence from cosmogenic isotopes and lake sediments: Geology, v. 26, no. 9, p. 835-838.
- Stokes, C. R., Tarasov, L., Blomdin, R., Cronin, T. M., Fisher, T. G., Gyllencreutz, R.,
  Hättestrand, C., Heyman, J., Hindmarsh, R. C. A., Hughes, A. L. C., Jakobsson, M.,
  Kirchner, N., Livingstone, S. J., Margold, M., Murton, J. B., Noormets, R., Peltier, W. R.,
  Peteet, D. M., Piper, D. J. W., Preusser, F., Renssen, H., Roberts, D. H., Roche, D. M.,
  Saint-Ange, F., Stroeven, A. P., and Teller, J. T., 2015, On the reconstruction of palaeoice sheets: Recent advances and future challenges: Quaternary Science Reviews, v. 125,
  p. 15-49.
- Stone, J. O., Balco, G. A., Sugden, D. E., Caffee, M. W., Sass, L. C., 3rd, Cowdery, S. G., and Siddoway, C., 2003, Holocene deglaciation of Marie Byrd Land, West Antarctica: Science, v. 299, no. 5603, p. 99-102.

885

886 887

888

889

890

891

892

898

899

900

901

902

903

907

- Stone, J. O., and Ballantyne, C. K., 2006, Dimensions and deglacial chronology of the Outer Hebrides Ice Cap, northwest Scotland: implications of cosmic ray exposure dating: Journal of Quaternary Science, v. 21, no. 1, p. 75-84.
- Stone, J. O., Ballantyne, C. K., and Fifield, L. K., 1998, Exposure dating and validation of periglacial weathering limits, northwest Scotland: Geology, v. 26, no. 7, p. 587-590.
- Stroeven, A. P., Harbor, J., Fabel, D., Kleman, J., Hattestrand, C., Elmore, D., Fink, D., and Fredin, O., 2006, Slow, patchy landscape evolution in northern Sweden despite repeated ice-sheet glaciation, *in* Willet, S. D., Hovius, N., Brandon, M. T., and Fisher, D. M., eds., Tectonics, Climate, and Landscape Evolution: Geological Society of America Special Paper 398, p. 387-396.
- Stroeven, A. P., Hättestrand, C., Kleman, J., Heyman, J., Fabel, D., Fredin, O., Goodfellow, B.
  W., Harbor, J. M., Jansen, J. D., Olsen, L., Caffee, M. W., Fink, D., Lundqvist, J.,
  Rosqvist, G. C., Strömberg, B., and Jansson, K. N., 2016, Deglaciation of Fennoscandia:
  Quaternary Science Reviews, v. 147, p. 91-121.
  Sugden, D. E., and Watts, S. H., 1977, Tors, felsenmeer, and glaciation in northern Cumberland
  - Sugden, D. E., and Watts, S. H., 1977, Tors, felsenmeer, and glaciation in northern Cumberland Peninsula, Baffin Island: Canadian Journal of Earth Sciences, v. 14, p. 2817-2823.
  - Tarasov, L., Dyke, A. S., Neal, R. M., and Peltier, W. R., 2012, A data-calibrated distribution of deglacial chronologies for the North American ice complex from glaciological modeling: Earth and Planetary Science Letters, v. 315-316, p. 30-40.
  - Tarasov, L., and Peltier, W. R., 2005, Arctic freshwater forcing of the Younger Dryas cold reversal: Nature, v. 435, no. 7042, p. 662-665.
- The IMBIE Team, 2020, Mass balance of the Greenland Ice Sheet from 1992 to 2018: Nature, v. 579, no. 7798, p. 233-239.

  Thompson, W. B., Dorion, C. C., Ridge, J. C., Balco, G., Fowler, B. K., and Svendsen, K. M.,
  - Thompson, W. B., Dorion, C. C., Ridge, J. C., Balco, G., Fowler, B. K., and Svendsen, K. M., 2017, Deglaciation and late-glacial climate change in the White Mountains, New Hampshire, USA: Quaternary Research, v. 87, no. 1, p. 96-120.
- Thompson, W. B., Fowler, B. K., and Dorion, C. C., 1999, Deglaciation of the northwestern
  White Mountains, New Hampshire: Physical and Quaternary Geography, v. 53, no. 1, p.
  59-77.
- 912 Ver Straeten, C. A., 2013, Beneath it all: bedrock geology of the Catskill Mountains and 913 implications of its weathering: Annals of the New York Academy of Sciences, v. 1298, p. 914 1-29.

- Vetter, L., Spero, H. J., Eggins, S. M., Williams, C., and Flower, B. P., 2017, Oxygen isotope
  geochemistry of Laurentide ice-sheet meltwater across Termination I: Quaternary
  Science Reviews, v. 178, p. 102-117.
- Walsh, G. J., and Ratcliffe, N. M., 1994, Preliminary bedrock geologic map of the Plymouth
   quadrangle and eastern portion of the Killington Peak quadrangle, Windsor and Rutland
   Counties, Vermont: United States Geological Survey and Vermont Geological Survey,
   scale 1:24,000.
- Winsor, K., Carlson, A. E., Caffee, M. W., and Rood, D. H., 2015, Rapid last-deglacial thinning
   and retreat of the marine-terminating southwestern Greenland ice sheet: Earth and
   Planetary Science Letters, v. 426, p. 1-12.
- Wright, S.F., 2018, Surficial Geology and Hydrogeology of the Bolton Mountain Quadrangle,
   Vermont Geological Survey Open File Report VG2018-4: Vermont Geological Survey.
- Zen, E. a., Goldsmith, R., and Hatch, N. L., 1983, Bedrock geologic map of Massachusetts:
   United States Geological Survey and Massachusetts Department of Public Works, scale
   1:250,000.